Published online 26 May 2017

Nucleic Acids Research, 2017, Vol. 45, No. 13 ***7807–7824***
doi: 10.1093/nar/gkx468

Phosphorylated SIRT1 associates with replication origins to prevent excess replication initiation and preserve genomic stability

Koichi Utani[1], Haiqing Fu[1], Sang-Min Jang[1], Anna B. Marks[1], Owen K. Smith[1], Ya Zhang[1], Christophe E. Redon[1], Noriaki Shimizu[2] and Mirit I. Aladjem[1,*]

[1]Developmental Therapeutics Branch, Center for Cancer Research, National Cancer Institute, National Institutes of Health, Bethesda, MD 20892, USA and [2]Graduate School of Biosphere Science, Hiroshima University, Hiroshima 739-8521, Japan

Received February 14, 2017; Revised May 09, 2017; Editorial Decision May 11, 2017; Accepted May 11, 2017

ABSTRACT

Chromatin structure affects DNA replication patterns, but the role of specific chromatin modifiers in regulating the replication process is yet unclear. We report that phosphorylation of the human SIRT1 deacetylase on Threonine 530 (T530-pSIRT1) modulates DNA synthesis. T530-pSIRT1 associates with replication origins and inhibits replication from a group of 'dormant' potential replication origins, which initiate replication only when cells are subject to replication stress. Although both active and dormant origins bind T530-pSIRT1, active origins are distinguished from dormant origins by their unique association with an open chromatin mark, histone H3 methylated on lysine 4. SIRT1 phosphorylation also facilitates replication fork elongation. SIRT1 T530 phosphorylation is essential to prevent DNA breakage upon replication stress and cells harboring SIRT1 that cannot be phosphorylated exhibit a high prevalence of extrachromosomal elements, hallmarks of perturbed replication. These observations suggest that SIRT1 phosphorylation modulates the distribution of replication initiation events to insure genomic stability.

INTRODUCTION

Genome duplication initiates at multiple sites, termed replication origins, and requires the assembly of pre-replication complexes (pre-RCs) that are further modified into pre-initiation complexes at the G1-S cell cycle phase transition (1–3). Insights into the roles of DNA sequence, chromatin structure and cis- and trans- acting factors in determining metazoan replication dynamics are key to a mechanistic understanding of how cells coordinate replication, transcription and chromatin condensation to insure genomic stability.

Recent genome-wide analyses have identified distinct DNA and chromatin modifications that modulate replication, and specifically, associate with replication origin activity (4–11). The assembly of pre-RCs, also known as replication licensing, renders chromatin available for the replication machinery but does not determine where and when DNA replication would initiate. Conversely, the association of replication origins with specific chromatin modifiers, although not strictly required for replication, correlates with the time and the location of replication initiation events. For example, early replicating origins associate with euchromatic histone modifications (H3K4me1/2/3, H3K9ac, H3K18ac, H3K36me3 and H3K27ac) (5), methylation of histone H4 lysine 20 by KMT5A (PR-SET7 or SET8) promotes loading of pre-RCs to chromatin (12) and the histone acetyltransferase HBO1 facilitates initiation of DNA replication (13). Chromatin modifications that affect replication initiation are not limited to euchromatin, as the H3K9 histone demethylase KDM4D, which acts on the heterochromatin mark H3K9Me3, facilitates replication initiation by enabling the recruitment of CDC45, a member of the replicative helicase (14). In another example, the histone methyl transferase DOT1L catalyzes H3K79 methylation that is associated with a group of replication origins, and this methylation prevents chromatin re-replication during a single cell cycle (4).

Chromosomes contain *cis*-acting elements that facilitate replication by affecting histone modifications (15–18). Such elements either colocalize with replication origins or inter-

*To whom correspondence should be addressed. Tel: +1 240 760 7312; Email: aladjemm@mail.nih.gov
Present addresses:
Owen K. Smith, Department of Biochemistry, Stanford University Medical School, 259 Campus Drive, Beckman B409, Stanford, CA 94305, USA.
Ya Zhang, George Washington University Cancer Center, George Washington University, Washington, DC, USA.
Koichi Utani, Department of Microbiology, Kanazawa Medical University, Uchinada Ishikawa 920-0293 Japan.

act with origins (19,20), creating a chromosomal context permissive for both transcriptional activity and replication initiation (21–23). However, it is unclear how specific histone modifications affect initiation frequency and regulate the rate of DNA synthesis. It also remains to be defined how signaling pathways (e.g. phosphorylation) target chromatin modifiers to modulate replication patterns.

SIRT1, an NAD^+ dependent deacetylase, is a member of the sirtuin family (24) and is homologous to the yeast Sir2, a transcriptional silencer. SIRT1 affects chromatin modifications, DNA damage/repair, aging, circadian rhythms, and metabolism (25,26). SIRT1 has been explored as a potential molecular target for the treatment of cancer (27,28). The yeast ortholog of SIRT1, Sir2, interacts with the ORC1 component of the pre-RC and binds replication origins (29). Mutations in Sir2 can activate initiation at a subset of yeast origins, suggesting that the acetylation state at replication origins might affect the formation of pre-RCs (30). In metazoa, emerging evidence suggests that metazoan SIRT1, like its yeast ortholog, also regulates DNA replication (31–34).

Mammalian SIRT1 is phosphorylated by several kinases including cyclinB/Cdk1 (35), JNK1 (36) and DYRK1-3 (37). Phosphorylation events on various residues have diverse effects. For example, phosphorylations of S27, S47, T530 and S682 affect intracellular localization, while phosphorylation of S682 induces transcriptional activity and apoptosis (36,38). Other phosphorylation sites (T530 and S540) mediate acetylation and affect cell cycle progression (37). Because the phosphorylation on T530 was reported to respond to oxidative stress and cell cycle perturbations (35,39), we have investigated the functional significance of SIRT1 phosphorylation on T530. Our findings suggest that the phosphorylated form of SIRT1 on Threonine 530 (T530-pSIRT1) binds chromatin in a cell-cycle specific manner. We further show that T530-pSIRT1 interacts with replication origins and plays a regulatory role in modulating the rate of DNA synthesis. The effects of SIRT1 depletion and temporal patterns of SIRT1 binding to replication origins suggest that SIRT1 inhibits initiation of some origins that are typically inactive during unperturbed cell cycles and are only activated when cells encounter potentially damaging conditions (dormant origins). Cells that do not contain T530-pSIRT1 (either because they are depleted of SIRT1 or because they contain a mutant form of SIRT1 that cannot be phosphorylated) exhibit elevated levels of DNA breakage, suggesting that T530-pSIRT1 associates with replication origins to modulate replication patterns and insure genomic stability.

MATERIALS AND METHODS

Cell lines and culture conditions

K562, HCT116, U2OS and MCF7 human cells were cultured in Dulbecco's modified Eagle's medium (DMEM, high glucose, GlutaMaxTM supplement, pyruvate, Invitrogen, 10569-010). Cells were cultured in a 37°C/5% CO_2 humidified incubator. For the induction of the Tet inducible elements, doxycycline was added to a final concentration of 2 μg /ml every 24 h. Cells were incubated for 36–72 h. For the induction of common fragile sites, a low dose of aphidicolin, 0.2 μM (final concentration), was added to cell cultures for 24 h.

Cell cycle fractionation by Elutriation

3×10^8 K562 cells were washed once with cold PBS- and separated by elutriation at each of the following flow speeds: 15 × 2, 16 × 2, 17 × 2, 18 × 2 19 × 2, 20 × 2, 21, 22, 23, 24, 25, 26, 28, 30, 35, 40, 45 and 50 ml/min. Each fraction was stained by PI/RNase in PBS- and run through FACS to determine cell cycle distributions.

Establishment of SIRT1 depleted cell lines

SIRT1 was depleted in HCT116, U2OS and MCF7 cells using CRISPR-CAS9. One 20-bp guide sequence targeting the first exon of SIRT1 (5′-GAGGCCGCGTCGTCCCCCGC-3′) was selected from a published database of predicted high specificity protospacer-PAM target sites in the human exome. Eurogins MWG Operon (Alabama, United States) synthesized two set of complementary oligonucleotides containing BbsI ligation adapters. Oligonucleotides were ligated into the BbsI-digested px330 vector (Addgene, 42229). The sequence of the construct was verified by sequencing using LKO.1 5′ primer. HCT116, MCF7 and U2OS cells were cultured in six-well dishes to 70–80% confluence for co-transfection with 2 μg of SIRT1 single guide RNA (sgRNA) plasmid, 2 μg of linearized pCR2.1 vector harboring a puromycin-resistance gene expression cassette, and 10 μl of Lipofectamine 2000 (Life Technologies) per well. The culture medium was changed 24 h after transfection and cells were incubated for another 24 h. Ten percent of transfected cells were used to seed 10-cm dishes in serial dilutions with medium, containing the indicated concentrations of puromycin for selection.

Plasmid construction

The FLAG-tag of pCMV tag2A plasmid was changed to a myc-tag. SIRT1 cDNA was obtained from K562 cells using ImProm-II™ Reverse Transcription System (Promega, A3800) and cloned into the HindIII/XhoI sites of pCMV myc tag2A vector by infusion kit (Clontech, 639645). Two PCR products with a mutation-inserted primer set were used to generate the mutant SIRT1 cDNA and were inserted into the HindIII/XhoI site of pCR2.1 vector using an infusion kit. These myc-tagged SIRT1 and mutant SIRT1 genes were transferred to the SalI/MluI sites of pTRE3G. Blasticidin resistance gene expression cassette was inserted to EcoRI/XhoI site of pTRE3G (Clontech)

siRNA transfection and inhibition of kinases

siRNA mediated inhibition was utilized to reduce the expression of endogenous DYRK1 (Invitrogen, HSS103011), DYRK2 (Invitrogen, HSS112282 or Invitrogen, HSS189079 or Qiagen, 1027410). AllStars negative control siRNA was purchased from Qiagen (Qiagen, SI03650318). siRNA transfection was performed using RNAiMax (Invitrogen, 13778030) with two or three repeated every 48 h. To determine kinase catalyzing SIRT1

T530 phosphorylation, the following kinase inhibitors were used: for DYRKs inhibition, Harmine (Sigma-Aldrich, 286044), (−)-Epigallocatechin gallate (Sigma-Aldrich, E4143) and CGP57380 (Sigma-Aldrich, C0993); for JNK1 inhibition, SP600125 (Sigma-Aldrich, S5567); for Cdk1 inhibition, RO-3306 (Sigma-Aldrich, SML0569). These inhibitors were added to HCT116 cells growing in 96-well plates with six different concentrations of each inhibitor, representing 125, 25, 5 times lower and 5, 25, 125 times higher than IC50. SIRT1 T530 phosphorylation levels were detected by T530-pSIRT1 antibody immunofluorescent staining (data not shown). Validations were performed by Western blots with each inhibitor at IC50 as shown in Figure 1 and in supplemental Figure S1.

Chromatin binding assays and western blotting

Chromatin binding assays were performed as previously described (40). Briefly, the cytoplasm fraction from 2×10^7 cells was isolated using a cytoplasmic extraction buffer (10 mM HEPES, 60 mM KCl, 1 mM EDTA, 0.075% (v/v) NP40, 1mM DTT and 1 mM PMSF, adjusted to pH 7.6). For tight chromatin binding assays, nuclei were isolated and further fractionated by sequential extractions with increasing salt concentrations (0.3, 0.45, 0.6, 1.2 and 1.8 M), 10 min each at 4°C with gentle rotation. Proteins in each fraction were immunodetected following SDS-PAGE. The following primary antibodies were used for western blots: anti-phosphorylated T530 SIRT1 (NCI153, currently available from Abcam, ab156585), anti-SIRT1 (Millipore, 07–131), anti-myc (Sigma, M4439), anti LaminB1 (SantaCruz, sc-6216), anti PCNA (SantaCruz #sc-7907), Anti-Topoisomerase (DNA) II Binding Protein 1 (Millipore, AB3245), anti-MCM2 (Cell Signaling, 3619S), anti-CDC7 (DDK) (Cell Signaling, 3603S), anti-Cdt1 (Cell Signaling, 8064S), anti-acetyl-Histone H4 (Lys16) (Millipore, 07–329), anti-ORC2 (BD BioScience, 559266), anti-Histone H3 (Millipore, 07-690), anti-RPA 70 kDa subunit (SantaCruz, sc-14696), anti-acetyl Lysine (Abcam, ab22550), anti DYRK1A (SantaCruz, sc-28899) and anti DYRK2 (SantaCruz, sc-130743). For secondary antibody, HRP linked anti-mouse IgG (Cell Signaling, 7076), HRP linked anti-rabbit IgG (Cell Signaling, 7074), HRP linked anti-goat IgG (SantaCruz, sc-2020) were used following the manufacturer's suggested protocol.

Kinase assays

DYRK2 proteins from the lysate of 5×10^7 cells were immunoprecipitated with an antibody against DYRK2 (Santa Cruz, sc-130743) using Sepharose beads (GE, 17-0885-01). Beads were washed three times with lysate buffer and once in PBS-, then resuspended in kinase assay buffer (10 mM HEPES pH 7.5, 50 mM NaCl, 10 nM $MgCl_2$, 10 mM $MnCl_2$, 1 mM EGTA, 1 mM dithiothreitol, 5 μM ATP, 10 mM NaF). Recombinant SIRT1 (Sigma, S8446), 20 μl of beads, and either 10 Ci of [γ-^{32}P] ATP or 1 mM ATP were used to evaluate kinase activity. Kinase reactions ran for 30 min to 3 h at 30°C. Reactions were stopped by the addition of SDS sample buffer. Samples were boiled for 5 min followed by SDS–PAGE, autoradiography and immunodetection.

In vitro SIRT1 deacetylation assay

SIRT1 deacetylation activity was measured using a SIRT1 deacetylation kit (Enzo life science, BML-AK555-0001). Myc-tagged SIRT1 variants including WT, T530A or T530E were expressed in SIRT1-depleted HCT116 cells and purified with a myc-specific antibody. Purified SIRT1 proteins were mixed with reaction components and substrate (p53AcK382) fluorometric signal was measured. After the addition of either the blank or NAD+ buffer, 0.5× SIRT1 substrate or 0.5× SIRT2 substrate were added to a 96-well plate with 5 μl volume of nuclei on ice. Following incubation for 30 min at 37°C, reactions were stopped by adding 5 μl of developer solution and an additional 10 min incubation at 37°C. The fluorometric signal was measured by Spectra Max GEMINIXS (Molecular Devices). The NAD^+ samples fluorometric values were normalized by subtracting the control values. EX527 was used to inhibit SIRT1 activity.

Chromatin immunoprecipitation

Chromatin immunoprecipitation was performed for phosphorylated T530 SIRT1, phosphorylated S139 MCM2 and acetylated H4K16 from wild-type HCT116 cells, using the ChIP Assay Kit (Millipore, 17-295) and following the manufacturer's protocol. Elutriated K562 cells were used for cell-cycle stage specific ChIP experiments. ChIP DNA (100 ng) was used as the template for amplification by random primer. Approximately 1 μg of DNA was sequenced using the method described below.

Nascent strand abundance assay

Replication origins were identified using the nascent-strand sequencing and abundance assay (41). In brief, DNA fractions (0.5-2 kb) were isolated using DNA fractionation on a 5–30% neutral sucrose gradient. 5′ single strand DNA ends were phosphorylated by T4 polynucleotide kinase (NEB, M0201S) and then with l-exonuclease (NEB, M0262S) to remove genomic DNA fragments that lacked the phosphorylated RNA primer. Single stranded nascent strands were random-primed using the Klenow and DNA Prime Labeling System (Invitrogen, 18187013). Double-stranded nascent DNA (1 μg) was sequenced using the Illumina genome analyzer II (Solexa).

Bioinformatics analysis

ChIP and nascent strands sequences were obtained by Illumina sequencing and aligned to the genome in the form of .BAM files as described (5,41). Sequences were converted to a BED file format using the Genomatix software. The BED formatted ChIP sequences were compared to BED formatted sequencing of genomic DNA, producing a BED file with 'peaks'. These peaks indicate where the sequences were enriched above background within the ChIP sample and above cell-type specific background.

For nascent strand peak finding, we used the SICER program with the following parameters: Window 200, Gap 600, and FDR 0.00001. The same parameters were used for ChIP-sequencing peak finding. H4K16Ac peaks were

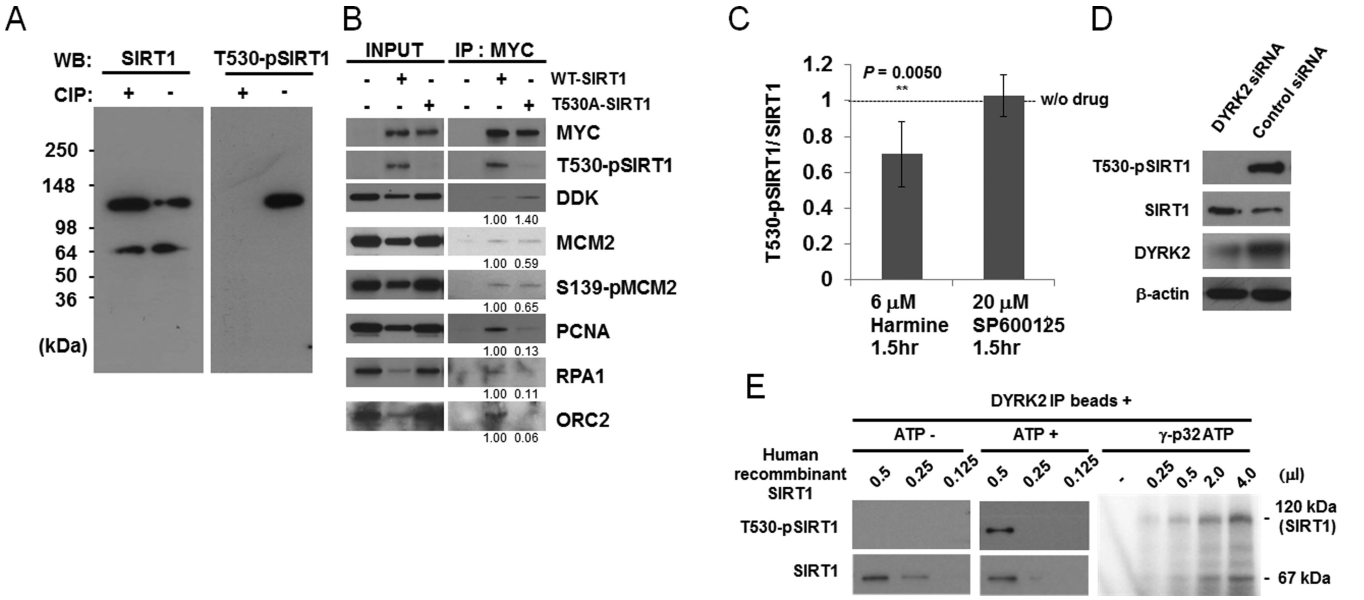

Figure 1. DYRK2 dependent T530 SIRT1 phosphorylation and molecular interactions. (**A**) Antibody characterization. Left, HCT116 cell extracts immunodetected with a monoclonal antibody recognizing the C-terminal of SIRT1 (pan-SIRT1). Right, HCT116 cell extracts immunodetected with a monoclonal antibody recognizing T530-pSIRT1. Extracts were incubated with or without alkaline phosphatase Calf Intestinal (CIP) at 37°C for 30 min prior to loading as indicated. The 64 kD form detected on the left two panels is a non-specific band associated with the pan-SIRT1 antibody. (**B**) HCT116 cells in which SIRT1 variant 1 was deleted were stably transfected with doxycycline induced myc-tagged WT SIRT1 or myc-tagged T530A-SIRT1. Following induction with doxycycline, proteins interacting with myc-tagged WT SIRT1 or myc-tagged T530A-SIRT1 were detected by co-immunoprecipitation with an antibody against the myc tag followed by immunodetection with the indicated antibody. The numbers under the panels represent the intensity ratios compared to the intensity of the signal in cells expressing SIRT1-WT. (**C**) T530-pSIRT1 detected in protein extracts from cells treated with the DYRK2 inhibitor harmine. The ratios between T530-pSIRT1 and pan-SIRT1 proteins are shown. The data are derived from three independent biological repetitions with duplicates. Original images are shown in supplemental Figure S1C. (**P value < 0.005). (**D**) T530-pSIRT1, SIRT1, DYRK2 and β-actin expression in HCT116 cells transfected with siRNA against DYRK2 or with a control siRNA. (**E**) DYRK2 immuneprecipitated from HCT116 cells was incubated with human recombinant SIRT1 with or without ATP (left panel) or with γ-p32 ATP (center panel) at 30°C for 3 h. SIRT1 phosphorylation levels were detected by either western blot (left and center panels) with T530-pSIRT1 antibody or radiograph of γ-p32 ATP (right panel).

identified using MACS2 broad peaks program. Randomized peaks files that contain the same number and sizes of peaks at random locations throughout the genome were created using a custom java script as previously published (5). Colocalization of nascent strand, protein-bound sequences, and histone-localized sequences were compared using java scripts, BedIntersect and BedSubtract, as previously described (5). The Genome Inspector program of Genomatix was also used to quantify features from colocalization. Correlations of each sequenced peaks within the 2, 5 and 10 kb windows were quantified and visualized for figures and tables included here.

Single fiber DNA replication profiling

Dynamic molecular combing and analysis was performed as previously described (42). Briefly, thymidine analogs, CldU and IdU, were integrated into replicating DNA for specific periods of time. DNA was spread across silanized slides and the incorporation of analogs was measured through detection of fluorescent secondary antibodies. Specifically, CldU (Accurate chemical, OBT0030), IdU (Becton Dickinson, 347580) and ssDNA antibodies (Chemicon, MAB3034) are detected by anti-rat IgG1 Alexa 647 (Invitrogen, A-21247), anti-mouse IgG1 Alexa 488 (Invitrogen, A-11029), and Rabbit anti-mouse IgG2a Alexa 350 (Invitrogen, A-21130) followed by anti-Rabbit IgG Alexa 350 (Invitrogen A-21068), respectively.

BrdU comet assays

The BrdU comet assay was performed to detect newly synthesized single strand DNA as previously described (42). Cells were labeled with 100 μM BrdU for 30 min. BrdU labeled cells were washed with PBS-, placed into fresh medium and incubated for an additional 30 min, 1 h or 2 h to mature replicating DNA strands. Labeled cells were collected, suspended in low-melting-point agarose and added to agarose-coated CometSlides. Slides were incubated in an alkaline lysis solution according to the manufacturer's protocol (Trevigen, 4250-050-K). Following electrophoresis, slides were neutralized by treatment with 0.4 M Tris–HCl, washed with PBS-, and immunostained. Incorporated BrdU substituted newly replicated DNA was detected with an anti-BrdU antibody (BD BioScience, 555627), followed by anti-mouse IgG Alexa 488 (Invitrogen, A-11029). DNA was counter-stained with DAPI and slides were dried according to the manufacturer's instructions (Trevigen, 4250-050-K). Digital images were acquired using a 20× objective lens on a BD pathway 855 microscope, which was controlled by AttoVision (Becton Dickinson). Images were analyzed by CometScore software (TriTeK).

Immunostaining and imaging analysis

HCT116 cells were labeled with EdU for 20 min, fixed by addition of 2% paraformaldehyde and permeabilized with

0.1% triton/PBS. EdU was detected by the Click-iT assay kit (Invitrogen, C10340), following the manufacturer's protocol. Subsequently, rabbit anti-T530-phosphorylated SIRT1 IgG was incubated with Alexa 488 conjugated anti-mouse IgG or Alexa 555 conjugated anti-rabbit IgG. A Zeiss LSM 780 confocal microscopy was used to take images under the following conditions: Lens—63×/1.40 oil lens DIC M27 (Plan-APOCHROMAT), pinhole—57 μM, image size—1816 × 1816. The stage within the S phase was identified by examining EdU labeling patterns (e.g. see supplemental Figure S6). EdU-labeled nuclei were individually analyzed using the co-localization function in Zeiss-Zen software; EdU/ T530-p-SIRT1 signals were extracted from the image and the number of colocalized-pixels were quantified.

Metaphase spread preparation

For metaphase spread preparation, cells were treated with 75mM KCl hypotonic buffer, then fixed with pre-chilled Carnoy fixation buffer. After three rounds of fixation with Carnoy fixation buffer, metaphase cells were spread onto water-layered slides and the metaphase-spread slides were dried. Slides were washed with PBS- and then counterstained with DAPI containing VectaShield Antifade (Vector, H-1000). Metaphase images were captured using an OLYMPUS IX70 (60×/1.40 oil Ph3 PlanApo, Retiga-SRV FAST1394) controlled by IPlab pathway 4.0. These images were analyzed with the ImageJ software.

Co-IP

Proteins associated with T530-pSIRT1 and myc-tagged SIRT1 mutants were immunoprecipitated using anti-T530-pSIRT1 or anti-myc antibody for myc-tagged SIRT1. 1.5×10^8 PBS-washed cells were treated with cytoplasmic extraction buffer (10 mM HEPES, 60 mM KCl, 1 mM EDTA, 0.075% (v/v) NP40, 1mM DTT and 1 mM PMSF, adjusted to pH 7.6.) for 10 min on ice, and the isolated nuclei gently washed once with NP40-free buffer. Protein complexes were cross-linked for 30 min on ice using the DSP crosslinker (Sigma, 22585) to fix protein interactions within 1.2 Å. The crosslinking reaction was stopped by addition of 10 mM Tris–HCl (pH 7.5), followed by three washes with PBS-. Since DSP crosslinks lysine residue, non-fixed cells were used for acetylated lysine immunoprecipitation. A proteinase inhibitor cocktail (Sigma P8430), phosphatase inhibitors (10 μM NaF, 2 μM Na_3VO_4) and 1 mM PMSF were added and samples were sonicated for three intervals of 5 s followed by 15 s on ice. After a 10-minute centrifugation at 14000 rpm/4°C, supernatants were transferred to new tubes with 4 μg of antibody to each sample. After rotation overnight at 4°C, 100 μl of Sepharose-beads were added and samples were incubated for an additional 1 h at 4°C, under rotation. The protein-bead complexes were collected by centrifugation at 6000g for 1 min and washed with PBS-/0.1% Triton and treated with 2 units DNase I (10 mM Tris–HCl, 2.5 mM $MgCl_2$, 0.5 mM $CaCl_2$, pH 7.6 in PBS–) at 37°C for 15 min. After centrifugation, pellets were washed three times with PBS–, and 50 μl 2× SDS sample loading dye was added. Samples were heated at 50°C for 15 min to elute proteins and 45 μl of eluted proteins were collected without beads. Proteins were denatured and decrosslinked by addition of 10 μM DTT and boiling for 10 min.

RESULTS

DYRK2 phosphorylates SIRT1 to facilitate chromatin and pre-replication complex binding

To characterize the role of SIRT1 phosphorylation, we developed an antibody that specifically recognized SIRT1 phosphorylated on threonine 530 (T530-pSIRT1). As shown in Figure 1A, this antibody detected T530-pSIRT1 and did not detect alkaline-phosphatase-treated SIRT1 (compare right and left lanes). To evaluate the role of SIRT1 T530 phosphorylation, we used a CRISPR-Cas9 expression vector to deplete and replace SIRT1 variant-1, the most prevalent splicing variant of SIRT1 (43), with a doxycycline-inducible myc-tagged SIRT1 (WT-SIRT1) or with a doxycycline-inducible myc-tagged SIRT1 harboring a threonine to alanine point mutation at position 530 (T530A-SIRT1), which could not be phosphorylated. As expected the phosphorylation-specific T530-pSIRT1 antibody did not detect T530A-SIRT1 (Figure 1B).

Because T530 SIRT1 phosphorylation was reported to vary with the cell cycle, we tested if T530-pSIRT1 specifically associated with proteins regulating DNA replication. We found that T530-pSIRT1 associated with the replication regulator Dbf4-dependent kinase (DDK), with the mini chromosome maintenance protein 2 (MCM2), its DDK-mediated phosphorylated form, S139-pMCM2 (44), the proliferating cell nuclear antigen (PCNA), the replication protein A (RPA) and ORC2, a member of the pre-RC (Figure 1B). Associations with the single-stranded DNA binding protein RPA and with PCNA, as well as with ORC2, were most noticeable in the WT SIRT1 cells. The non-phosphorylable mutant T530A-SIRT1, which interacted more strongly with DDK, exhibited the same level of interactions with MCM and its derivative and a marked decrease in association with PCNA, RPA and ORC2. This observation might suggest that T530A is recruited on pre-RCs at a low level or might reflect slower replication and increased initiation frequency in cells harboring this mutation (see below).

To determine which kinase is responsible for the phosphorylation of SIRT1 on T530, a kinase inhibitor screen was performed. Harmine, a pan-DYRK inhibitor, markedly reduced T530 SIRT1 phosphorylation (Figure 1C). We also tested inhibitors targeting JNK1 (36) and cyclinB1/CDK1 (35) since those proteins have been previously reported to phosphorylate human SIRT1, and DYRK1A/ DYRK3 kinase inhibitors since DYRK1A/3 kinases have been reported to phosphorylate the murine SIRT1 on the orthologous amino acid T522 (37,43). The CDK1 inhibitor RO-3306, the DYRK1A inhibitor epigallocatechin gallate (EGCG), the DYRK3 inhibitor CGP57380, and the JNK-1 inhibitor SP600125 did not inhibit T530 phosphorylation significantly (Figure 1C and Supplemental Figure S1A–C). In agreement with these observations, siRNA-mediated DYRK2 depletion reduced T530-pSIRT1 (Figure 1D), whereas depletion of DYRK1A did not significantly

alter T530-pSIRT1 levels (Supplemental Figure S1D). Further studies demonstrated that DYRK2 could phosphorylate recombinant His-tagged SIRT1 on T530 *in vitro* (Figure 1E).

T530-pSIRT1 was detected in both the cytoplasm and the nucleus during interphase (supplemental Figure S2A and B). In mitotic cells, SIRT1 detached from mitotic chromosomes before metaphase and was re-recruited to chromatin following cytokinesis (Supplemental Figure S2C). Cells that expressed the non-phosphorylable T530A-SIRT1 exhibited lower accumulation of myc-SIRT1 on the tight chromatin bound fraction (Supplemental Figure S2B; compare elutions at 0.6 M and 1.2 M NaCl), indicating that phosphorylation of T530 promotes the association of SIRT1 to chromatin. In cell cycle fractionated (elutriated) K562 cells (Figure 2A), levels of nuclear soluble and chromatin-bound T530-pSIRT1 (but not cytoplasmic T530-pSIRT1) peaked during the gap phases (G1 and G2) and were reduced during S-phase (Figure 2B–D), consistent with the observation that T530-pSIRT1 associated with chromatin during the assembly of pre-replication complexes but not during replication. These results suggested that SIRT1, and in particular, T530-pSIRT1, associated with chromatin during the preliminary step of DNA replication initiation.

To determine if phosphorylation on T530 affected SIRT1 deacetylation activity, we measured deacetylation activity *in vitro* using the p53AcK382 peptide substrate, using SIRT1 depleted cells (SIRT1 KO) as a baseline (Supplemental Figure S3A). Cells that expressed the non-phosphorylable T530A-SIRT1 exhibited lower deacetylase activity than the activity measured in cells that expressed the WT SIRT1. We also tested the deacetyation activity in a T530E-mutant, which mimicked phosphorylated SIRT1. Deacetylation activity in this mutant was restored almost to the levels exhibited by WT SIRT1. In concordance, SIRT1 depletion in HCT116 cells led to an increase in overall protein acetylation, which was partially reduced by the expression of SIRT1 derivatives (Supplemental Figure S3B).

T530-pSIRT1 is highly enriched at replication initiation sites but not at actively elongating replication forks

Since SIRT1 appeared to be associated with proteins involved in the initiation of DNA replication, we assessed the extent of T530-pSIRT1 binding to replicating chromatin (elongating replication forks) and replication initiation sites (replication origins). We performed chromatin immunoprecipitation followed by sequencing (ChIP-Seq) using the anti-T530-pSIRT1 antibody in colon carcinoma HCT116 cells (Figure 3) and in cell cycle fractionated chronic myelogeneous leukemia K562 cells (Supplemental Figure S4A and B; for example screenshots, see Figure 3A and Supplemental Figure S4C). We then compared the locations of T530-pSIRT1 binding sites with those of replication initiation sites delineated by nascent DNA strand accumulation (5,41). The results demonstrated that T530-pSIRT1-associated with the majority of replication initiation sites. For example, in HCT116 cells, T530-pSIRT1-associated replication initiation sites represented 88.7% of all replication origins (Figure 3B). Notably, 80.4% of T530-pSIRT1 binding sites colocalized with nascent DNA (Supplemental Figure S5A, rightmost column). This observation suggests that the phosphorylated form of SIRT1 preferentially but not exclusively associated with replication initiation sites.

Since some of T530-pSIRT1 binding sites did not colocalize with replication origins, we were wondering if there were other chromatin features that distinguish origin-associated T530-pSIRT1 binding sites from T530-pSIRT1 binding sites that were not associated with origins. We therefore determined the association of these two groups of T530-pSIRT1 binding sites with histone H3 trimethylated on lysine 4 (H3K4Me3) and histone H3 acetylated on lysine 27 (H3K27ac), which are enriched in replication origins, and histone H3 monomethylated on lysine 4 (H3K4Me1), which does not exhibit enrichment in replication origins (5). As shown in Figure 3C, T530-pSIRT1 binding sites that colocalized with origins were enriched in H3K4Me3 and H3K27ac, whereas the T530-pSIRT1 binding sites that did not colocalize with origins were not enriched in those chromatin marks. Because replication origins often associate with transcription start sites (TSS), we tested if chromatin-bound T530-pSIRT1 sites associated with TSS. Both T530-pSIRT1 sites and replication origins exhibited a high level of association with TSS, consistent with previous reports (5,41), but the association was stronger in T530-pSIRT1 binding sites that also colocalized with replication origins: nearly 50% of origin-associated T530-pSIRT1 binding sites colocalized within 2 kb of TSS whereas less that 30% of T530-pSIRT1 binding sites that did not associate with origins exhibited colocalization within 2 kb of TSS (Figure 3D).

We used ChIP-sequencing to map the chromatin interactions of H4K16Ac, a SIRT1 substrate, and of the DDK substrate S139-pMCM2 (44) (Figure 4 and supplemental Figure S5B; See Supplemental Figure S4C for examples of IGV screenshots). Sequencing in asynchronous HCT116 cells yielded a total of 230956 peaks in H4K16Ac-associated sequences and 151932 peaks in S139-pMCM2 associated sequences (Figure 4). ChIP-Seq peaks denoting protein-DNA interactions with S139-pMCM2 and H4K16Ac also exhibited a marked colocalization with replication origins (Figure 4A and B). Sequencing in asynchronous HCT116 cells yielded a total of 230 956 peaks in H4K16Ac-associated sequences and 151 932 peaks in S139-pMCM2 associated sequences (Figure 4C). All origins colocalized with H4K16Ac bound regions and 67 876 (86.1%) origins colocalized with S139-pMCM2 bound regions (Figure 4C). These correlations were not observed when we performed the same analysis using randomized ChIP-seq data (Figure 4B).

As shown in supplemental Table S1A, T530-pSIRT1 colocalized with 91% of the replication origins (52690/57873 peaks) that were likely to be shared with other cancer cells (5), while it colocalized with only 16.4% of cell-type specific origins (216/1319 peaks), which initiated replication only in HCT116 and not in other cancer cell lines. Similarly, S139-pMCM2 binding sites preferentially correlated with shared replication initiation sites whereas H4K16Ac colocalized with both shared origins (56 683/57873 peaks, 97.9%) and cell type-specific origins (1062/1319 peaks, 80.5%). These observations suggested that T530-pSIRT1 binding regions and S139-pMCM2 binding regions were primarily shared origins, whereas

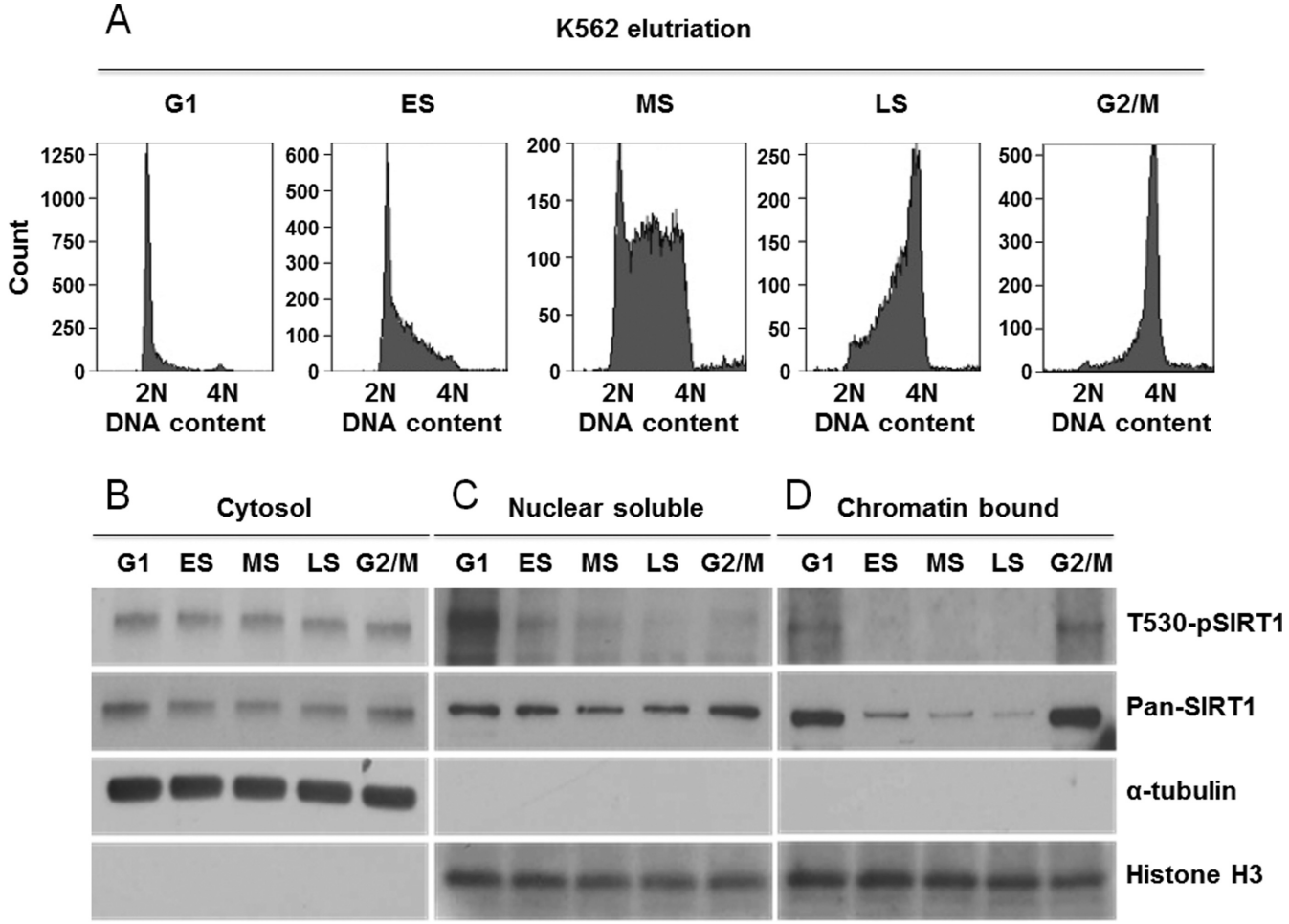

Figure 2. Cell cycle modulated cellular distribution of T530-pSIRT1. (**A**) K562 cell cycle specific fractions were collected by elutriation. DNA content distribution of fractions corresponding to G1 (G1), early (ES), middle (MS) and late (LS) S-phase and G2/M (G2/M). (B–D) From each cell cycle fraction, T530-pSIRT1, pan-SIRT1, α-tubulin and Histone H3 and were detected in cytosol (**B**), nuclear soluble (**C**) and chromatin bound fractions (**D**). Three individual experiments were performed and representative results are shown.

H4K16Ac colocalized with all origins. These correlations were not observed when analyses were performed using randomized files (Supplemental Table S1B).

To understand the dynamics of SIRT1 interactions with replication origins, we performed T530-pSIRT1 ChIP-Seq in cell-cycle fractionated K562 cells, which are amenable to reverse synchrony by elutriation (Supplemental Figure S4A). An analysis of the extent of genome-wide colocalization with specific replication origins initiating in early, middle and late S-phase (Supplemental Figure S4B) demonstrated that the extent of colocalization of T530-pSIRT1 binding sites with replication origins varied through the cell cycle (Figure 4D and Supplemental Figure S5C). T530-pSIRT1 binding was most prominent during the G1 phase and the late S-phase, concurring with the immunoblot analysis of T530-pSIRT1 (see Figure 2D). However, T530-pSIRT1 binding sites strongly associated with origins that replicated during the middle and late S-phase, and the association of T530-pSIRT1 binding sites with early-replicating origins was weaker (Figure 4D). As shown in Supplemental Figure S5A, the association of T530A-SIRT1 with origins was weaker (61.6% of T530A-SIRT1 peaks associated with origins) compared to the origin association of T530 pSIRT1 peaks and T530E-SIRT1 (88.7% and 90.8% respectively). These observations are in line with the suggestion that the T530-pSIRT1 associates with replication origins prior to the initiation of DNA replication, and that the phosphorylation on T530 is required for this association.

To evaluate whether T530-pSIRT1 also localized at actively replicating DNA, we compared the patterns of T530-pSIRT1 foci with replication factories, nuclear structures containing multiple regions that undergo DNA replication simultaneously in HCT116 cells (Supplemental figure S6). Replication factories were distributed in the nucleus in a punctate pattern (replication foci) and could be visualized by labeling cells with the thymidine analog EdU. The patterns of replication foci varied through the S-phase with typical patterns delineating early, middle and late S-phase (for examples of typical patterns, see supplemental Figure S6A). We compared the intensity of both EdU-labeled replication foci and T530-pSIRT1 foci throughout the S-phase (supplemental Figure S6B) and measured the frequency of colocalization between T530-pSIRT1 and EdU labeled foci (Supplemental Figure S6C). Although the frequency of colocal-

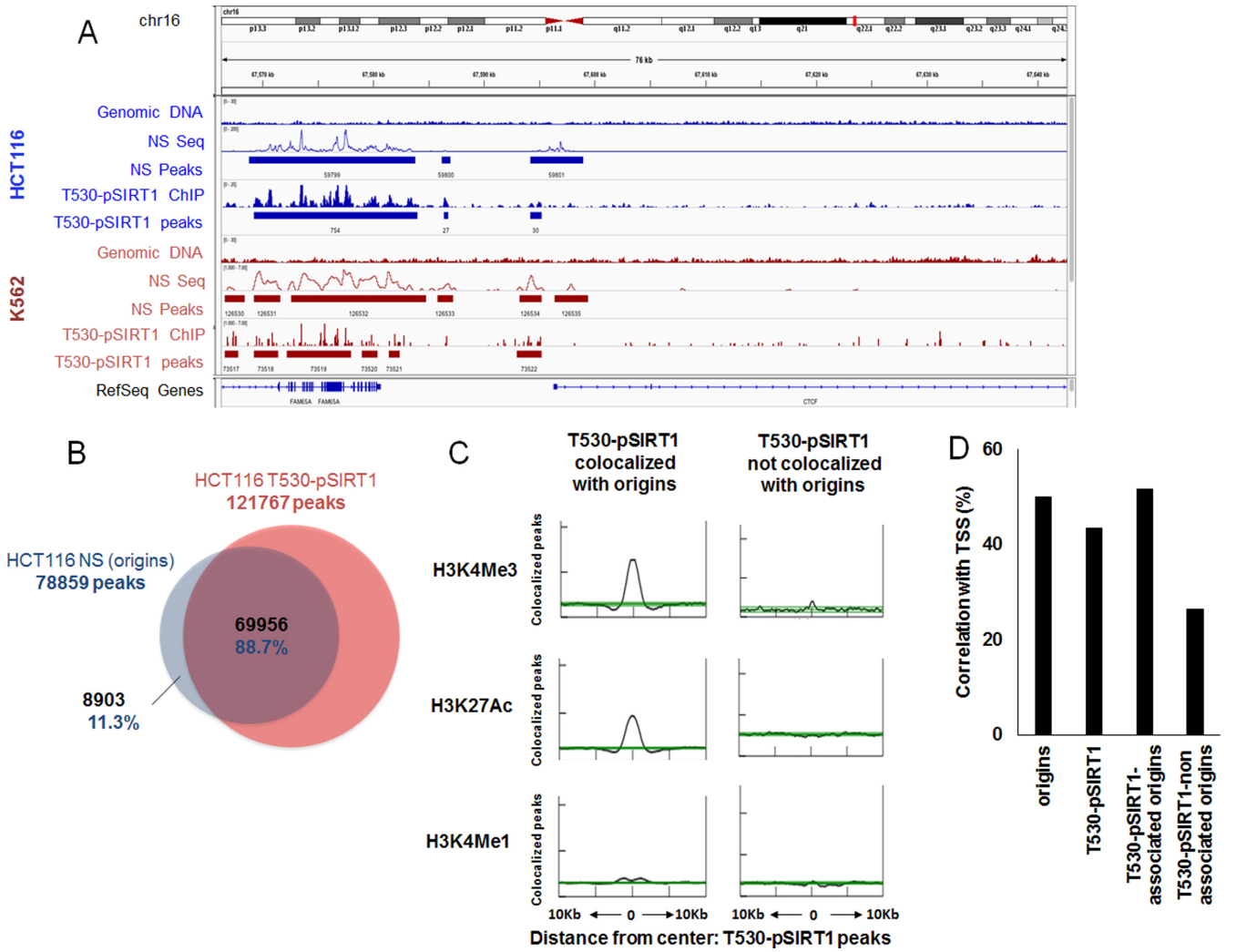

Figure 3. T530-pSIRT1 is associated with replication origins. ChIP-seq using the antibody recognizing T530-pSIRT1 (Figure 1) was performed in parallel with nascent strand abundance sequencing (NS-Seq) to map replication origins in HCT116 and K562 cells. (**A**) IGV viewer screenshots aligning T530-pSIRT1 ChIP-Seq with NS-Seq (replication origin peaks). A representative genomic location adjacent to the CTCF gene, encompassing both an origin-rich and an origin-poor region, is shown. Top panel shows an ideogram of the chromosome above a ruler showing chromosomal coordinates. Tiled reads (tdf) and peaks called against genomic DNA (bed) data are shown below the coordinates. Genetic features (RefSeq) are shown under the tdf and bed data. (**B**) Colocalization of T530-pSIRT1 binding sites (ChIP-Seq) and replication initiation sites (NS-Seq) in HCT116 cells. The total numbers of peaks for T530-pSIRT1 ChIP-seq and NS-Seq, the numbers (black) and the fractions (blue) of each group of origins (origins associated with T530-pSIRT1 and origins taht did not associate with T530-pSIRT1) are indicated. See supplemental Figure S5A for additional analyses. (**C**) Colocalization of T530-pSIRT1 binding sites with chromatin modifications H3K4Me3, H3K27ac and H3K4Me1. Left, a histogram analyzing colocalization of chromatin marks with replication origins associated T530-pSIRT1 binding sites; right, a histogram analyzing colocalization of chromatin marks with T530-pSIRT1 binding sites that are not associated with replication origins. Each histogram depicts the number of colocalizing histone modification (H3K4Me3, H3K27ac or H3K4Me1) peaks as a function of the distance from the center of T530-pSIRT1 peaks. The extent of colocalization, noted in each histogram, is measured as the fraction of peaks within 10 kb of the histone modification. (**D**) Graph depicting the percentage of colocalization between transcription start sites (TSS) in HCT116 cells and replication origins (NS-seq), T530-pSIRT1 peaks, T530-pSIRT1 peaks associated with origins and T530-pSIRT1 peaks not associated with origins. 2 kb windows were used for the analysis.

ized EdU and T530-pSIRT1 foci was somewhat higher at the earliest stage of S-phase, replication factories did not exhibit major colocalization with T530-pSIRT1 foci at any stage of S phase.

SIRT1 phosphorylation affects the pace of DNA replication

We next asked whether phosphorylation of SIRT1 on T530 affected DNA replication patterns. Single-fiber analyses of thymidine analog (CldU, IdU) incorporation during DNA replication (Figure 5A) demonstrated that inter-origin distances decreased in HCT116 cells depleted of SIRT1 and in cells harboring the T530A mutant, but not in the cells complemented with the WT SIRT1 or the phospho-mimetic mutant T530E (Figure 5B). The rate of replication fork elongation, reflected in the length of replication tracks, was slower in cells depleted of SIRT1 and significantly slower in cells harboring the T530A mutant but not in cells harboring the T530E mutation (Figure 5C). However, cells containing either T530A SIRT1 or T530E SIRT1 contained a high

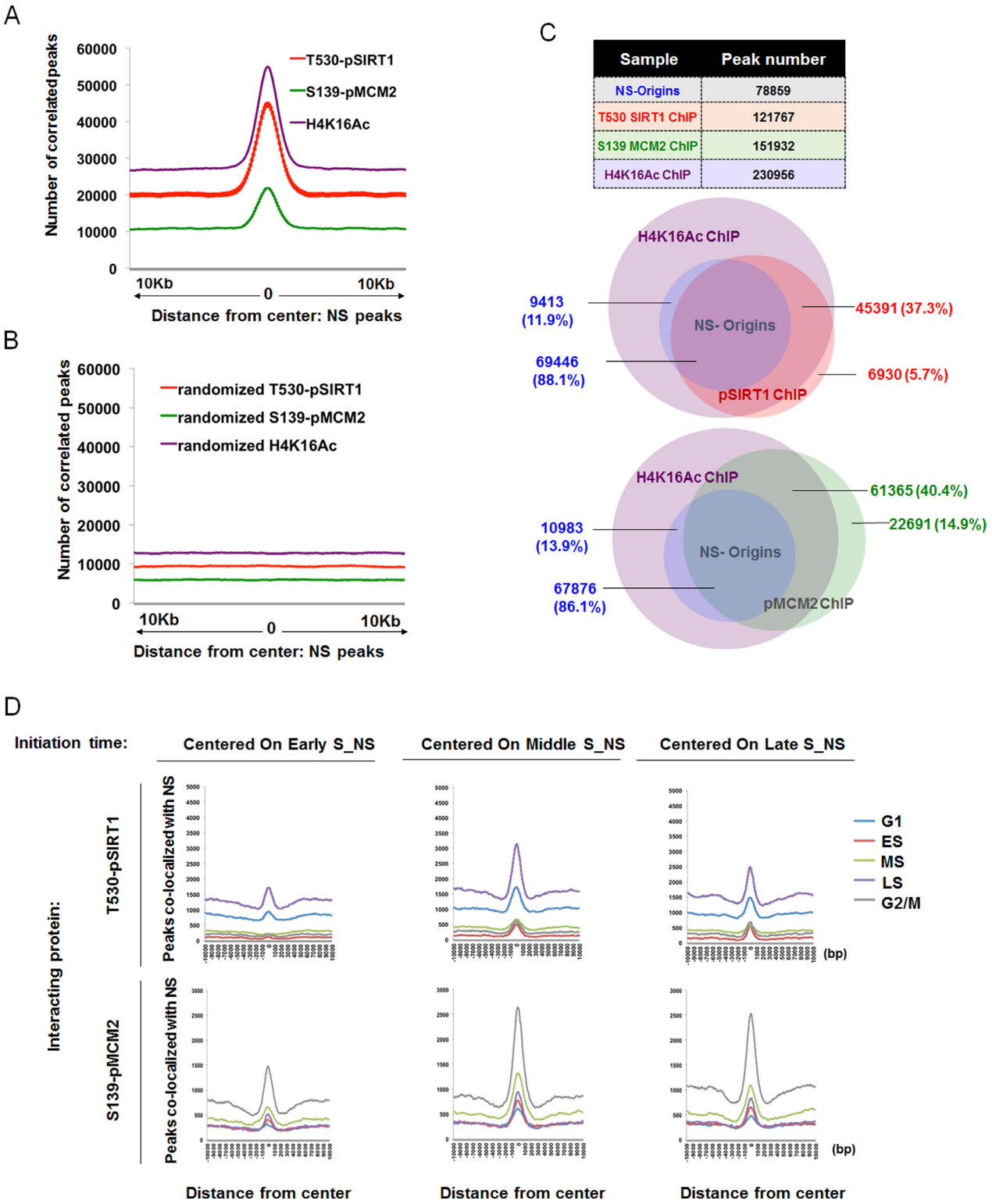

Figure 4. Replication origins colocalization with H4K16Ac, T530-pSIRT1 and S139-pMCM2. (**A**) The distributions of T530-pSIRT1, S139-pMCM2 and H4K16Ac binding sites aligned with the replication origins HCT116 cells. The histogram depicts the number of colocalizing T530-pSIRT1 peaks as a function of the distance from the center of NS-Seq peaks. Correlation frequencies are summarized in supplemental Table S2. (**B**) Extent of colocalization for randomized ChIP-Seq peaks of T530-pSIRT1, S139-pMCM2 and H4K16Ac with HCT116 nascent strand peaks. (**C**) The Venn diagrams show colocalization of NS-Seq, T530-pSIRT1 ChIP-Seq and H4K16Ac ChIP-Seq (top) or NS-Seq, S139-pMCM2 ChIP-Seq and H4K16Ac ChIP-Seq (bottom). The table shows the number of peaks called for each NS-Seq or ChIP-Seq experiment. (**D**) ChIP-seq with antibodies against T530-pSIRT1 and S139-pMCM2 were performed in cell cycle fractionated K562 cells (G1, early (ES), middle (MS), late (LS) S-phase and G2/M (G2/M)). The extent of genome-wide colocalization with replication origins initiating in early, middle and late S-phase is illustrated as the number of correlating ChIP-Seq peaks vs. the distance from NS-Seq peaks. Data are summarized in supplemental Table S3.

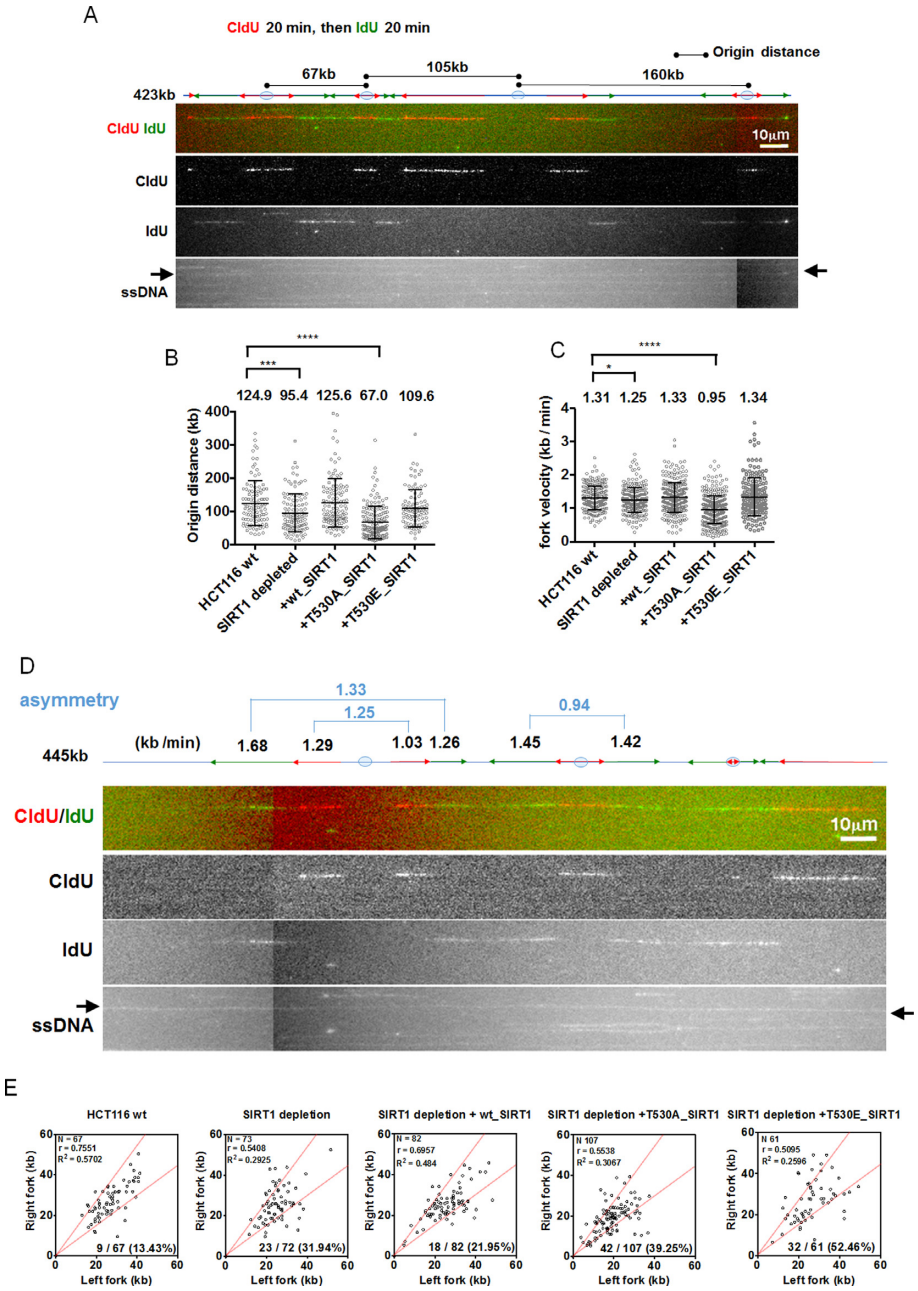

Figure 5. T530-pSIRT1 affects the pace of DNA Replication. SIRT1 depleted HCT116 cells and derivatives containing doxycycline-induced SIRT1, T530A SIRT1 and T530E SIRT1 were exposed to doxycycline for 3 days and then labeled with CldU, followed by IdU for 20 min each. Newly replicated DNA fibers were stretched on microscope slides and visualized using antibodies against ssDNA (blue), CldU (red) and IdU (green). (**A**) An example of replication initiation patterns identified by CldU/IdU patterns. Arrows point to the DNA fiber (ssDNA) with replication signals. 67, 105 and 160 kb indicate distances between 3 origins. (**B**) Replication origin distances calculated as shown in panel A. (**C**) Replication fork velocities calculated as the length of ongoing replication forks divided by the IdU or CldU labeling time. (**D**) An example of replication fork length asymmetry measurements and calculations. (**E**) Asymmetry rates were calculated by comparing the length of labeled tracks traveling from each origin to the left vs to the right. Asymmetric forks were defined as forks emanating from a single origin with a left fork to right fork ratios larger than 1.33 or smaller than 0.75. Arrows point to the DNA fiber (ssDNA) with replication signals. The fraction of asymmetric forks is shown at the bottom right corner inside each dot plot. Data shown are combined results from two independent biological experiments for each cell line (*P value < 0.05, ***$P < 0.005$, ****$P < 0.001$.)

fraction of asymmetric replication forks, which often reflect replication fork stalling (Figure 5D,E).

Since a markedly short inter-origin distance was observed in cells harboring T530A-SIRT1, we asked whether those additional replication origins differed from the origins activated in cells harboring WT SIRT1. Nascent strand abundance in cells expressing the WT and the T530A mutant (Figures 6 and 7A) revealed that both SIRT1-depleted and T530A SIRT1-expressing cells exhibited a dramatically increased number of replication initiation sites (NS-Seq peaks) when compared to cells expressing WT SIRT1 (110 052 and 103 976 peaks in SIRT1 depleted and T530A mutant cells respectively *vs.* 78859 peaks in WT SIRT1). SIRT1-depleted cells complemented with WT SIRT1 had initiation sites similar to those of the WT (74 481 peaks in SIRT1 depleted cells complemented with WT SIRT1 versus 78 859 peaks in WT SIRT1. The number of NS-Seq peaks also increased in cells harboring the phosphomimetic T530E mutant, but this gain did not translate to a shortened inter-origin distance (Figure 5), suggesting that cells harboring T530E-SIRT1 exhibited a higher flexibility of origin utilization without increasing the frequency of initiation. Taken together, these observations imply that the phosphorylation of T530 SIRT1 might suppress the activation of a group of potential replication origins.

We asked if replication origins suppressed by SIRT1 corresponded to a class of origins, termed 'dormant' origins, which are known to be induced upon perturbation of DNA replication or in cells exhibiting mutations in genes regulating DNA replication (20,45,46). To identify a population of dormant replication origins, we first compared the distribution of NS-Seq peaks from HCT116 cells to the distribution of NS-Seq peaks HCT116 cells exposed to a low dose of aphidicolin (APH) for 24 hours and released in APH-free medium for 24 h. Exposure to APH resulted in slow progression through S-phase, and cells reinstated a normal cell cycle distribution after 24 h of growth without APH (Figure 6A). However, the first S-phase after release from APH-mediated inhibition resulted in a marked increase in the number of initiation sites (gained NS peaks) detected by NS-Seq (96 998 peaks in APH-treated WT HCT116 cells versus 78 859 peaks in WT HCT116 cells; Figure 6A and B). As shown in Figure 6B, only 61.5% of the replication origins detected in HCT116 cells that were exposed to APH and released (empty purple-outlined circle) corresponded to replication origins in HCT116 that were not exposed to APH (light blue-filled circle). By contrast, NS-Seq in SIRT1 depleted cells detected 110 052 replication origins (grey-filled circle), and 89.1% of those active origins colocalized with replication origins detected in cells exposed to APH and released (Figure 6C). In agreement, cells complemented with SIRT1 contained fewer replication origins (74 481 peaks) than SIRT1 depleted cells (110 052) and cells complemented with T530A-SIRT1 (103 976 peaks). Also in agreement, only 64.2% of replication origins active in cells complemented with SIRT1 (violet-filled circle) colocalized with active replication origins from cells that were exposed to APH and released (Figure 6D) whereas 86.3% of active replication origins in cells complemented with T530A SIRT1 (pink-filled circle) colocalized with active replication origins from cells that were exposed to APH and released (Figure 6E; for screenshots, Figure 7A). The gained NS peaks, which corresponded to activated dormant replication origins (those origins that were inactive in cells harboring intact SIRT1 but initiated replication either in APH treated cells or in SIRT1 depleted cells), were located in genomic regions that associated with T530-pSIRT1 in cells harboring WT SIRT1 (Figure 7B). Such colocations were not observed when using randomized files for APH and SIRT1 gained peaks. These results suggest that T530-pSIRT1 associated with either active or dormant origins, and that the dormant origins were able to start replication in the absence of T530-pSIRT1, or in cells with T530-pSIRT1 undergoing replication stress.

The activation of additional origins observed in SIRT1 depleted cells and in cells harboring T530A SIRT1 was accompanied by slow replication. To understand the underlying cause of this activation, we used BrdU-comet assays to determine if the slow rate of DNA synthesis reflected differences in the rate of replication elongation. Short newly replicated DNA maturation rates were directly measured in the original and SIRT1 depleted clones, as well as in depleted clones complemented with WT SIRT1, T530A SIRT1 and T530E SIRT1 (Figure 8A and B). All cells contained immature DNA fragments that were not incorporated into high molecular weight DNA within 30 min after pulse BrdU labeling for 30 min (Figure 8C). However, only in cells expressing the T530A mutation, the BrdU-comet assay detected many cells with immature DNA fragments that were not incorporated into high molecular weight DNA one hour after release from BrdU labeling (Figure 8B and C). The short DNA fragments are not visible in all cells after a chase period of 2 h, suggesting that DNA synthesis in cells harboring the T530A mutation was slowed but not halted. Such immature nascent strands were not detected in cells harboring WT SIRT1 or the phospho-mimetic T530E mutation, suggesting that the T530A mutation elicits slow maturation of the lagging strands during DNA replication.

Phosphorylation of SIRT1 on T530 affects genomic stability and generation of extrachromosomal elements

Although SIRT1 and T530-pSIRT1 associated with replication origins and their absence affected initiation frequency and the pace of DNA replication, cells continued to proliferate without SIRT1 or with T530A SIRT1. We investigated if the absence of SIRT1, the inability to phosphorylated SIRT1 or the presence of the phospho-mimetic T530E mutation could affect markers of chromosomal instability induced by perturbation of DNA replication. Metaphase chromosome spreads were prepared from WT, HCT116 SIRT1 depleted cells and SIRT1 depleted cells reconstituted with WT SIRT1, T530A SIRT1 and T530E SIRT1 that were exposed to APH, then released into fresh medium with colcemid and allowed to proceed to mitosis (Figure 9A). Cells that were exposed to APH and allowed to proceed to mitosis contained an increased frequency of chromosome breakage (Figure 9B, red dots) and extrachromosmal DNA elements (Figure 9B, blue dots). The frequency of DNA breaks increased in cells depleted of SIRT1 and in cells harboring the T530A SIRT1 and T530E mutations (Figure 9B). These observations suggest that the SIRT1 plays a role in prevent-

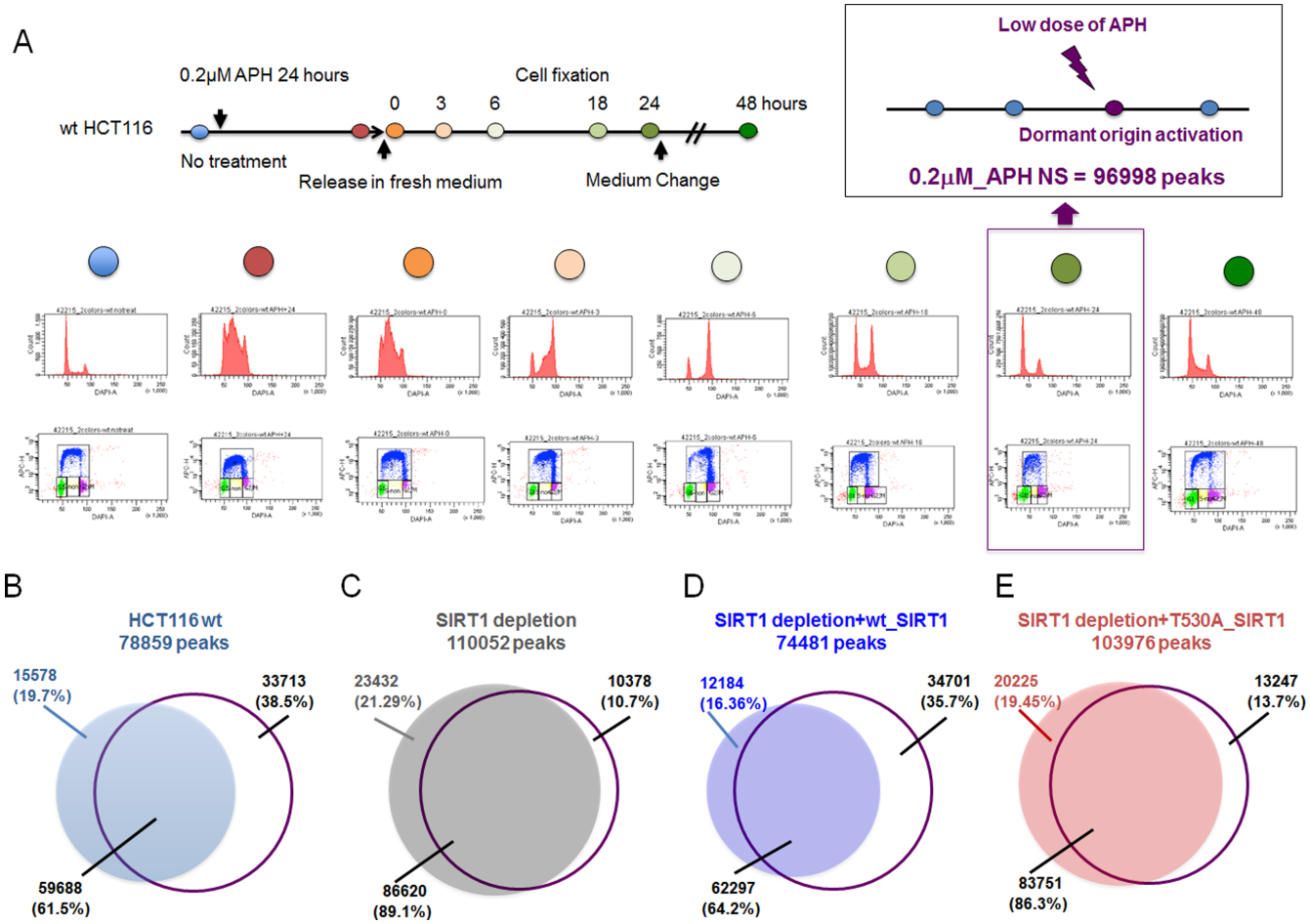

Figure 6. Cells with SIRT1 depletion or with T530A-SIRT1 activate dormant origins. (**A**) HCT116 cells were exposed to a low dose (0.2 μM) of aphidicolin for 24 hours, then released into fresh media without aphidicolin for up to 48 h. Cell cycle progression was monitored by 2D FACS using EdU incorporation and DNA content. Cells released in aphidicolin-free medium for 24 h were collected for NS-seq. The more origin peaks suggested dormant origin activation with low dose of APH. (B–E) Sequencing of nascent strands prepared from HCT116 cells transiently exposed to aphidicolin for 24 h and released in aphidicolin-free medium for 24 h. Venn diagrams showing the extent of nascent strands colocalization between aphidicolin-treated cells (empty purple-outlined circle) and (**B**) untreated cells, light blue-filled circle; (**C**) SIRT1 depleted cells, gray-filled circle; (**D**) SIRT1 depleted cells complemented with WT SIRT1, violet-filled circle and (**E**) and SIRT1 depleted cells complemented with T530A SIRT1, pink-filled circle.

ing DNA breakage and maintenance of genomic stability, and that the ability to phosphorylate and dephosphorylate SIRT1 in T530 is required for this function.

DISCUSSION

In this study, we found that T530-pSIRT1 associated with chromatin, bound preferentially to DNA replication origins and associated with pre-RC complex components and replication fork components. While the SIRT1 substrate, H4K16Ac, associated with both replication origins and non-origin regions, T530-pSIRT1 exhibited a higher preference for origins. Although T530-pSIRT1 associated with origins, the association with T530-pSIRT1 was not essential for genome duplication as cells could proliferate without SIRT1 or with T530A-SIRT1. The majority of the T530-pSIRT1 binding sites (80%) were localized at origins, and those origins also exhibited a marked association with transcription start sites and other histone modifications, H3K4Me3 and H3K27ac. The other T530-pSIRT1 binding sites, which did not associate with H3K4Me3, did not initiate replication during unperturbed growth. When SIRT1 variant-1 was depleted and/or replaced with a T530A mutant that could not be phosphorylated, cells exhibited slow replication and activated dormant origins, indicating that T530-pSIRT1 either facilitated fast replication or prevented initiation from the group of dormant replication origins. Cells harboring the phospho-mimetic T530E-SIRT1 exhibited replication dynamics similar to those of cells harboring WT-SIRT1, supporting the notion that the requirement for phosphorylation of SIRT1 is required for the maturation of nascent strands. Notably, although SIRT1 depleted cells continue to proliferate in culture, cells without SIRT1 phosphorylation on T530 as well as the constitutive phosphorylation mimic T530E-SIRT1 exhibited high incidences of chromosome breakage and extra chromosomal elements, suggesting that both SIRT1 phosphorylation and dephosphorylation are involved in the faithful maintenance of genomic stability.

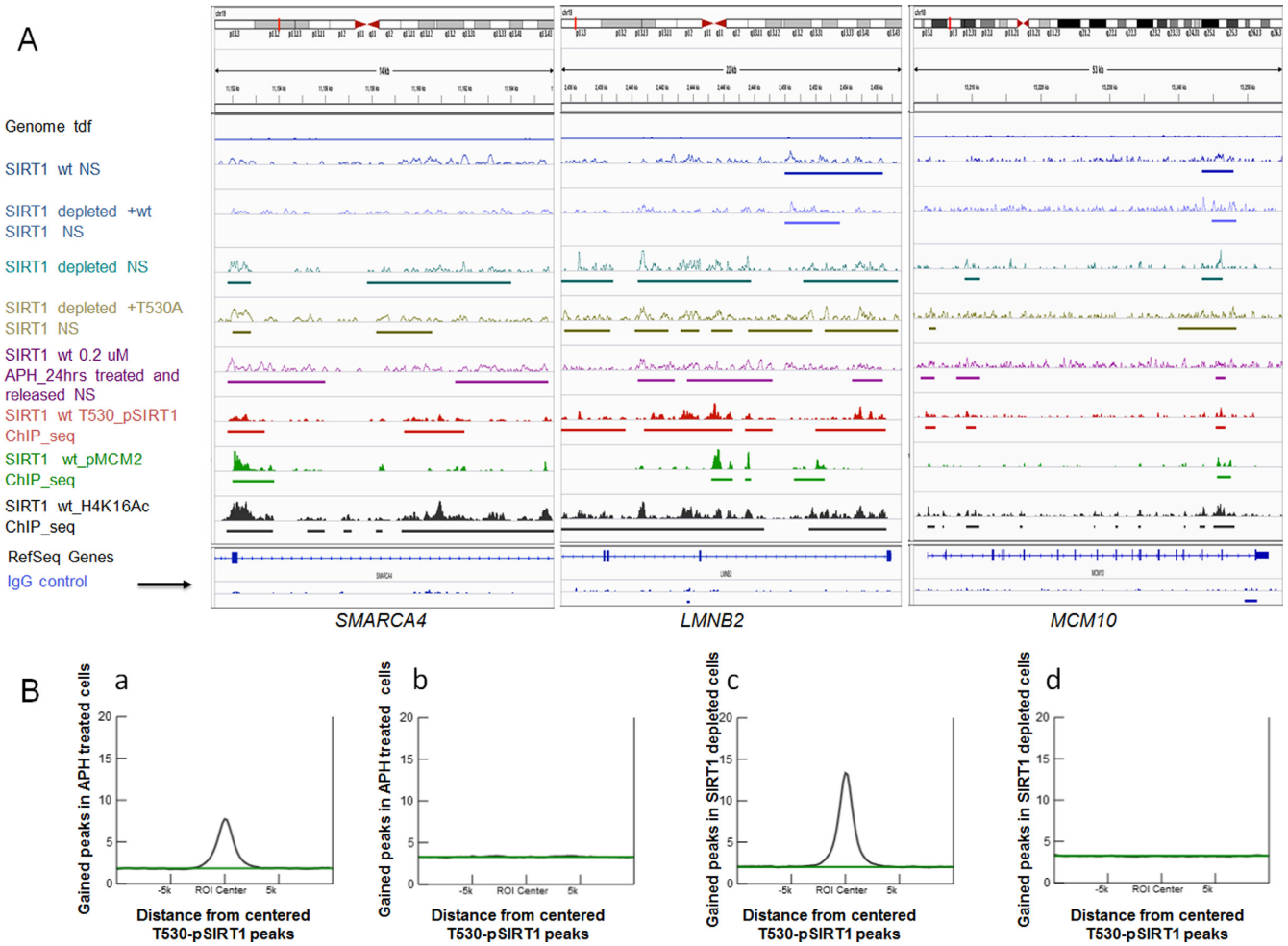

Figure 7. Genome-wide location of dormant origins. (**A**) Screenshot examples of dormant origins activation in SIRT1 depleted and T530A SIRT1 HCT116 cells. For each locus, the distribution of tiled reads (TDF) aligned to that region is shown above the called peaks (BED files) in the same region. (**B**) Colocation analysis of T530-pSIRT1 bound regions to (a) APH-gained origins, (b) randomized APH-gained origins, (**c**) SIRT1-depleted gained origins and (**d**) randomized SIRT1-depleted gained origins. Windows were centered on peaks from T530-pSIRT1 ChIP-Seq considering a 20 kb window size (72).

SIRT1 T530 is phosphorylated by DYRK2 (Dual specificity tyrosine phosphorylation-regulated kinase 2), a kinase involved in cell growth and differentiation. The phosphorylation of the murine SIRT1 by DYRK1A and DYRK3 at T522 is considered homologous to SIRT1 T530 in humans (43). Because the deacetylation activity is compromised in the T530A mutant, we cannot exclude the possibility that the ability to suppress dormant origin activation necessitates both origin binding and deacetylase activity. Our results did not exclude the possibility that, under certain circumstances, DYRK2 mediated phosphorylation could play a parallel role in human cells. DYRK2 is a well conserved enzyme (47) that is involved in diverse biochemical interactions including cell cycle progression (48,49) and in developmental processes including epithelial to mesenchymal transition (50). Interestingly, DYRK2 also interacts with the ubiquitin ligase network by acting as a scaffold for the EDVP complex, which contains EDD/UBR5, DDB1 and VPRBP (51). Our recent studies have demonstrated another link between the ubiquitin machinery, including DDB1, and a subgroup of replication origins via RepID, a DDB1-Cul4 associated protein (7). These observations suggest that DYRK2 might act in multiple ways to regulate the initiation of DNA replication, modulating both the ubiquitin ligation machinery and the phosphorylation of SIRT1.

T530-pSIRT1 associates preferentially with origins that initiate replication in middle and late S-phase. T530-pSIRT1 associates with these origins during the gap phases and not during the S-phase of the cell cycle and does not colocalize with replication foci beyond early S-phase. These observations suggest that T530-pSIRT1 binds to potential replication origins prior to initiation of DNA replication and not during the replication process. The timing of SIRT1 association with origins may explain why SIRT1 was not detected in iPOND-based nascent strand binding protein assays (47,52). The association with origins but not with elongating replication forks is in agreement with its interactions with TOPBP1, an origin binding protein (33), and with MCM10, a CDK substrate (53). We did not observe an interaction between SIRT1 and MCM10 but since MCM10 travels with replication forks, specific interactions at origins might have been diluted and not detected. The observed in-

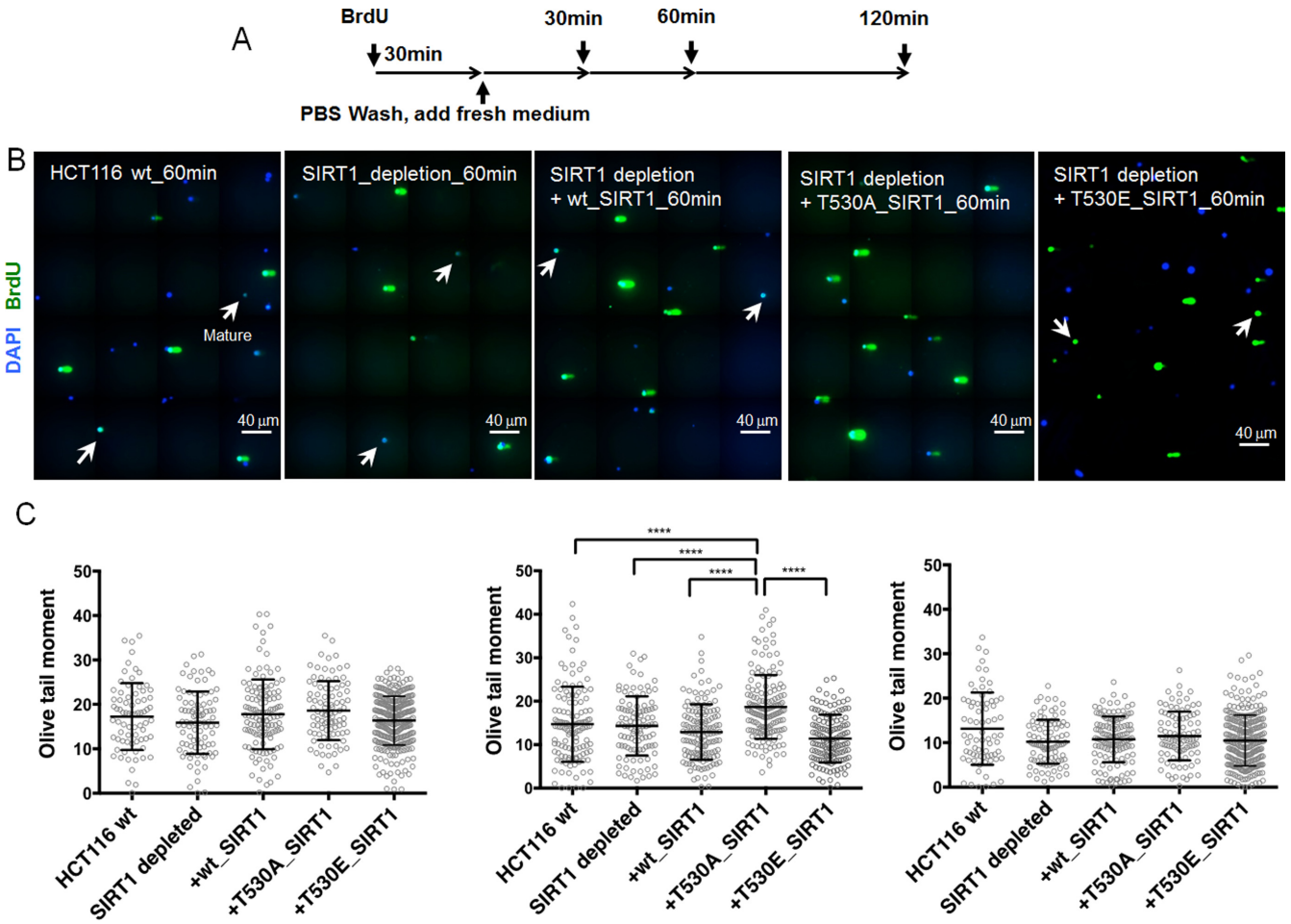

Figure 8. T530-pSIRT1 is required for nascent strand maturation Replicating DNA in HCT116 cells and derivative clones was labeled by BrdU incorporation for 30 min. Cells were then washed three times in PBS- and released in fresh media for another 30, 60, 120 min each ($N > 100$, results from two independent biological experiments at each time point). The extent of maturation of BrdU-containing DNA fragments was detected by alkaline BrdU-comet assay. Olive tail moment was calculated using the following formula: [(tail.mean – head.mean) × tail %DNA/100] as described in the methodology section. Statistical analyses were performed using a Mann–Whitney test. (**A**) Experimental workflow. (**B**) Representatives images captured at the 60 min release time points for each cell line as indicated. Nuclei with completed replication signals are marked with white arrows. (**C**) Summaries of olive tail moment distributions at 30 (left), 60 (middle) and 120 (right) min (****P value < 0.001; ns = not significant).

crease in active initiation sites when SIRT1 is absent or mutated is also consistent with the hypothesis that SIRT1 binds potential origins prior to initiation and helps prevent initiation of DNA replication in about half of those potential origins.

Previous studies have reported preferential association of replication origins with chromatin modifying enzymes. For example, euchromatic histone modifications including methylation of H3K4 and acetylations of H3K9, H3K18 and H3K27 associate with early replicating origins, whereas heterochromatin-associated H3 and H4 hypoacetylation and H3K9 and H3K27 methylation (5,54,55) and the heterochromatin-associated ORCA/LRWD1 protein (56) colocalize with late replicating origins. The importance of chromatin in origin specification has also been recently demonstrated *in vitro* (57,58). Our data show that H4K16Ac, the target of SIRT1 deacetylation, colocalizes with replication origins but also associates with non-origin regions whereas T530-pSIRT1 exhibits a much higher preference to origins. These observations are in line with the role of HBO1, an H4K16Ac acetyl transferase, in the co-activation of the replication licensing factor CDT1 (59) and in H3K14 acetylation around TSS to activate nearby replication origins (9). Deacetylation by SIRT1 can also impact histone methylation, which in turn affect origin activity. For example, pre-RC recruitment can be facilitated by methylation of histone H4 lysine 20 (12) by KMT5A, through an interaction with the bromo-adjacent homology (BAH) domain of ORC1 (12,60), and by KDM4D mediated reduction of the H3K9me3 levels (14). Consistent with a role in genome organization, origin associations with chromatin modifications vary with cell differentiation status (5,54,55) and might reflect coordination between replication and transcription. Chromatin modifications can also play a negative regulatory role, for example, prevention of re-replication at a subgroup of replication origins by association with H3K79me2 (4). These observations provide a precedent for the putative role of T530-pSIRT1, which binds the majority of replication origins, in preventing initiation from replication origins that are not concomitantly

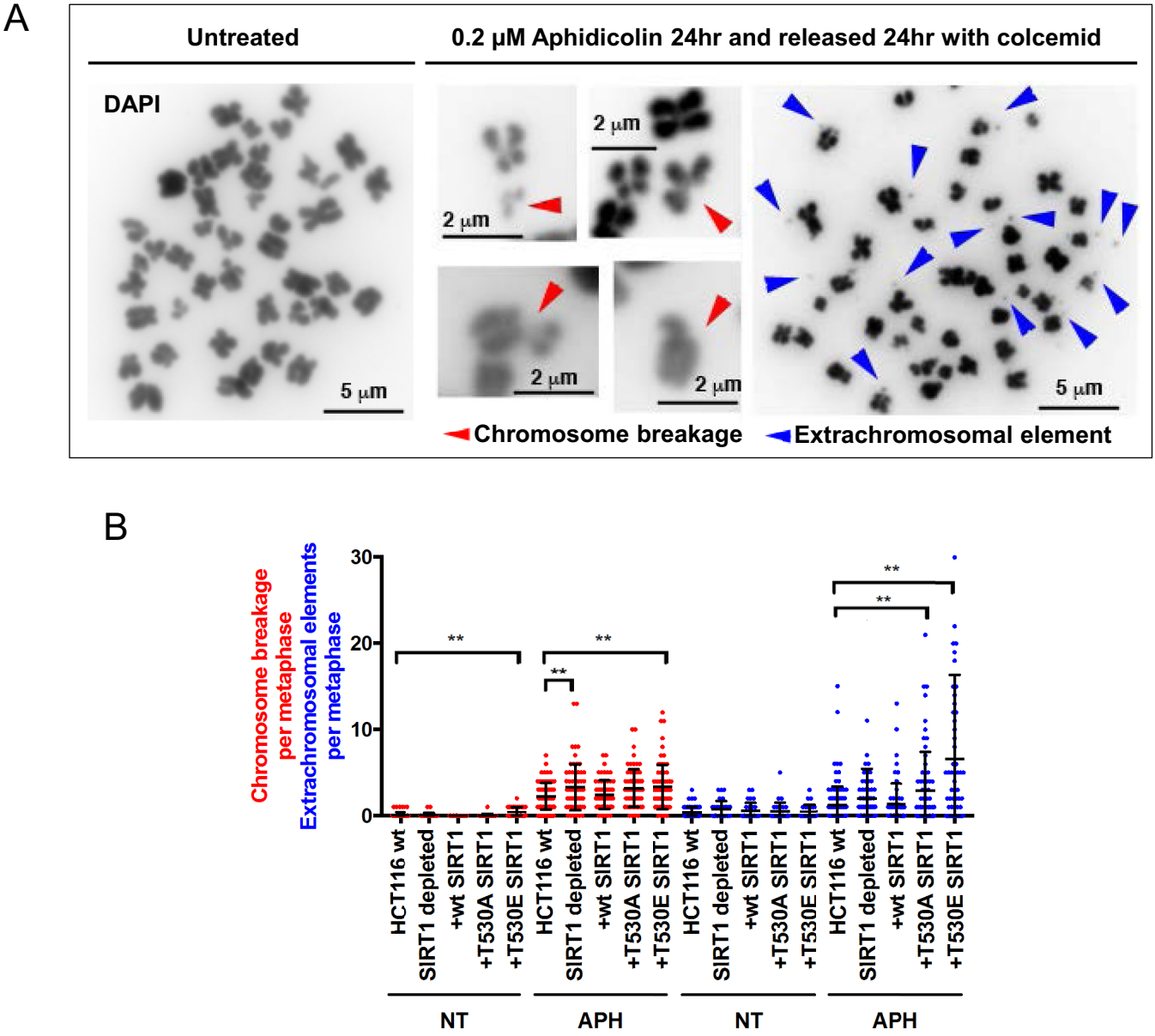

Figure 9. Chromosome fragility and extrachromosomal elements in HCT116 and derived SIRT1 mutant cells. HCT116 cells were exposed to a 0.2 μM of aphidicolin for 24 h, then released into fresh medium containing colcemid for 24 h. (**A**) Representative images of metaphase spreads from untreated cells and from aphidicolin treated cells are shown. Chromosome breakage points (red arrows) and extrachromosomal elements (blue arrows) are marked. (**B**) HCT116 cells, HCT116 cells with a SIRT1 deletion, and HCTT116 cells with a SIRT1 deletion complemented with dox-inducible WT-SIRT1, T530A SIRT1 or T530E SIRT1 were treated with doxycycline for 3 days and transiently exposed to aphidicolin as described in (A). The incidence of DNA breakage and extrachromosomal elements is shown as red and blue dot, respectively. Over 30 metaphase spreads were analyzed for each cell line. Data are compiled from two independent biological experiments (**$P < 0.01$, ***$P < 0.005$).

associate with H3K4Me3. As modeled in Figure 10, our observations are consistent with a model whereby T530-pSIRT1 alters chromatin structure to prevent initiation during normal growth and that this process is alleviated by H3K4Me3.

Replication initiation frequency varies in a cell-type specific manner during unperturbed growth (3,8,22,61) and the excess potential origins, which do not normally initiate replication, can be activated in response to cell cycle perturbations (45,62,63). The excess origins, however, are essential for maintaining genomic stability as is evident from the slow replication and loss of genomic stability that occur when the number of potential origins is reduced. For example in a mouse model harboring a mutation in the replicative helicase MCM4 subunit (63) and human RepID-depleted cells, which do not initiate replication from a proportion of origins (7). The results reported here suggest that SIRT1 activity is essential this process of origin choice. The slow replication patterns and increased initiation activity detected in cells harboring the T530-pSIRT1 mutant are consistent with a role of SIRT1 in maintaining genomic stability in case of direct perturbation of replication. The shortening

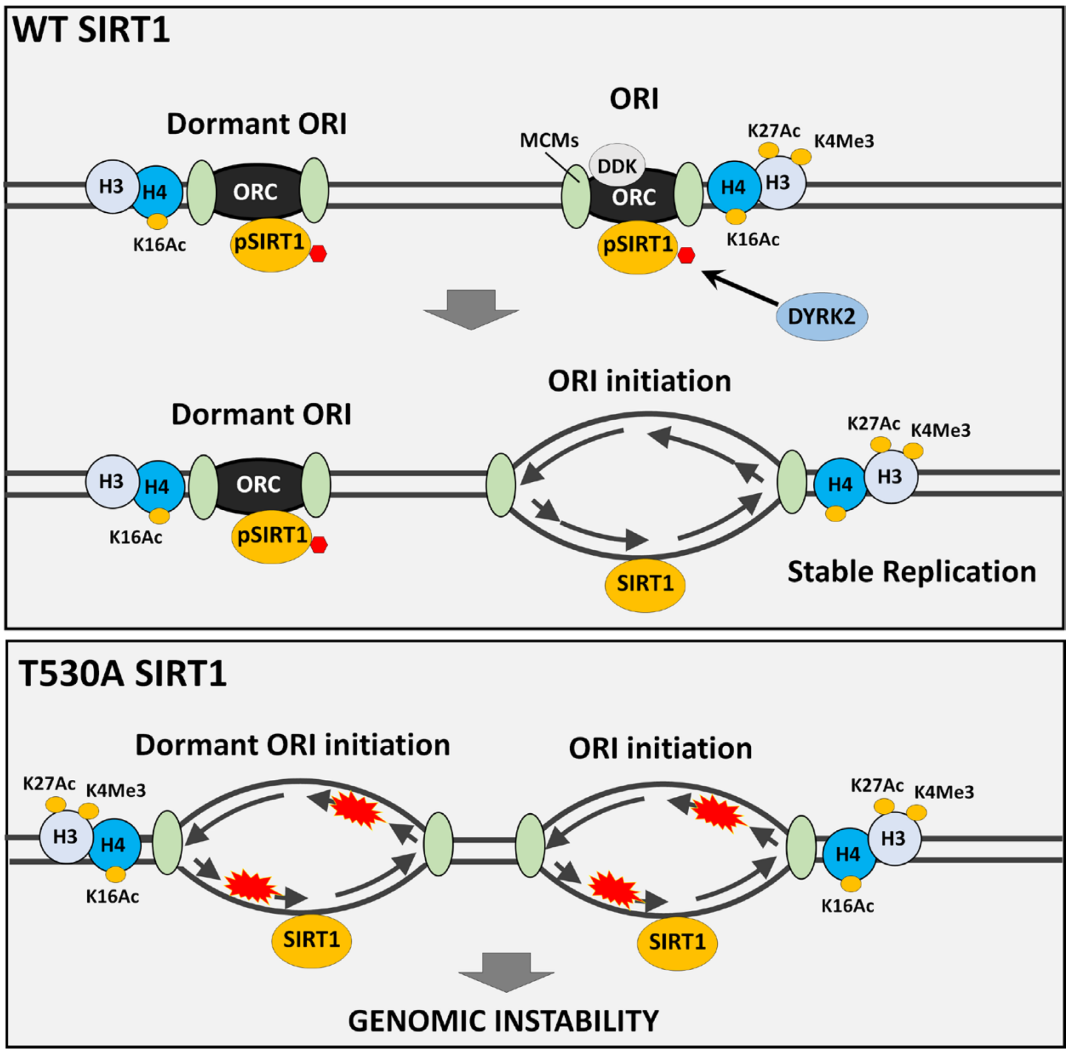

Figure 10. Role for T530-pSIRT1 in DNA replication. *Top panel*, a model of replication origin interactions with T530-pSIRT1 during unperturbed cell cycles. T530-pSIRT1 binds origins prior to initiation of DNA replication and inhibits initiation of DNA replication from a group of 'dormant' origins. Active origins are marked with H3K4 methylation and H3K27 acetylation whereas dormant origins, which also bind T530-pSIRT1, do not associate with methylated H3K4. *Bottom panel*, cells containing the T530A mutant activate dormant origins. The association between dormant origin activation, slow replication and chromosome breakage suggests that SIRT1 phosphorylation may also be involved in maintaining genomic stability.

of inter-origin distances and the associated slowing of DNA synthesis rates were markedly more prominent in SIRT1 depleted cells, suggesting a possible dominant negative effect of SIRT1 phosphorylation.

The increased frequency of DNA breakage and extrachromosomal elements observed in SIRT1 depleted and in cells harboring either T530A SIRT1 or T530E SIRT1 suggest that although SIRT1 is not essential for cell growth in culture, it plays a role in maintaining genomic stability. These observations are in line with a role for SIRT1 in cancer prevention, metabolism and aging. Notably, SIRT1 depletion in mice affects viability in a strain-specific manner and mice born without SIRT1 exhibit defects consistent with perturbed replication, such as small size, developmental defects and sterility (64). Mice mutated in SIRT1 can also exhibit impaired DNA damage response and genomic instability (65,66), and SIRT1 transgenic mice that moderately overexpress the protein exhibited lower levels of DNA damage (67). In addition, SIRT1 can act indirectly by affecting epithelial to mesenchymal transition (68) and plays a prominent role in the controlled proliferation of the hematopoietic lineage (69). SIRT1 was also shown in *Xenopus* to be required for replication fork stability (53). Because dormant origin activation and slow replication fork progression are thought to be essential for timely completion of whole genome duplication (70,71), interactions at SIRT1-suppressed origins in stem cells during perturbed growth might account for the variable effects of SIRT1 on aging and genomic stability. Taken together, our observations imply that SIRT1 T530 phosphorylation may act as a modulator of replication origin choice, helping to repress origin activity during normal chromosome duplication to avoid overactivation of replication origins while preventing situations that might lead to DNA breakage and genomic instability when cells are subject to cell cycle perturbations.

ACCESSION NUMBERS

All the nascent strand sequencing and ChIP sequencing data used in this study has been uploaded to GEO: GSE94403, GSE80298 and GSE80391.

SUPPLEMENTARY DATA

Supplementary Data are available at NAR Online.

ACKNOWLEDGEMENTS

We thank Dr Sandra Burkett for kindly performed karyotyping and SKY FISH and the CCR sequencing facility for their help in sequencing and analyzing ChIP-Seq and NS-Seq data. This study was supported by the Intramural Research Program of the NIH, Center for Cancer Research, National Cancer Institute and by fellowships from the Uehara Memorial Foundation and JSPS Research Fellowship for Japanese Biomedical and Behavioral Researchers at NIH.

FUNDING

Intramural Research Program of the NIH, Center for Cancer Research, National Cancer Institute [1ZIABC010411]; Uehara Memorial Foundation and JSPS Research Fellowship for Japanese Biomedical and Behavioral Researchers at NIH. Funding for open access charge: The intramural program of the Centre for Cancer Research, National Cancer Institute [1ZIABC010411], US National Institutes of Health.
Conflict of interest statement. None declared.

REFERENCES

1. Yeeles,J.T., Deegan,T.D., Janska,A., Early,A. and Diffley,J.F. (2015) Regulated eukaryotic DNA replication origin firing with purified proteins. *Nature*, **519**, 431–435.
2. Duronio,R.J. and Xiong,Y. (2013) Signaling pathways that control cell proliferation. *Cold Spring Harb. Perspect. Biol.*, **5**, a008904.
3. Fragkos,M., Ganier,O., Coulombe,P. and Mechali,M. (2015) DNA replication origin activation in space and time. *Nat. Rev. Mol. Cell Biol.*, **16**, 360–374.
4. Fu,H., Maunakea,A.K., Martin,M.M., Huang,L., Zhang,Y., Ryan,M., Kim,R., Lin,C.M., Zhao,K. and Aladjem,M.I. (2013) Methylation of histone H3 on lysine 79 associates with a group of replication origins and helps limit DNA replication once per cell cycle. *PLoS Genet.*, **9**, e1003542.
5. Smith,O.K., Kim,R., Fu,H., Martin,M.M., Lin,C.M., Utani,K., Zhang,Y., Marks,A.B., Lalande,M., Chamberlain,S. *et al.* (2016) Distinct epigenetic features of differentiation-regulated replication origins. *Epigenet. Chromatin*, **9**, 18.
6. Cayrou,C., Ballester,B., Peiffer,I., Fenouil,R., Coulombe,P., Andrau,J.C., van Helden,J. and Mechali,M. (2015) The chromatin environment shapes DNA replication origin organization and defines origin classes. *Genome Res.*, **25**, 1873–1885.
7. Zhang,Y., Huang,L., Fu,H., Smith,O.K., Lin,C.M., Utani,K., Rao,M., Reinhold,W.C., Redon,C.E., Ryan,M. *et al.* (2016) A replicator-specific binding protein essential for site-specific initiation of DNA replication in mammalian cells. *Nat. Commun.*, **7**, 11748.
8. Marks,A.B., Smith,O.K. and Aladjem,M.I. (2016) Replication origins: determinants or consequences of nuclear organization? *Curr. Opin. Genet. Dev.*, **37**, 67–75.
9. Feng,Y., Vlassis,A., Roques,C., Lalonde,M.E., Gonzalez-Aguilera,C., Lambert,J.P., Lee,S.B., Zhao,X., Alabert,C., Johansen,J.V. *et al.* (2016) BRPF3-HBO1 regulates replication origin activation and histone H3K14 acetylation. *EMBO J.*, **35**, 176–192.
10. Goldar,A., Arneodo,A., Audit,B., Argoul,F., Rappailles,A., Guilbaud,G., Petryk,N., Kahli,M. and Hyrien,O. (2016) Deciphering DNA replication dynamics in eukaryotic cell populations in relation with their averaged chromatin conformations. *Sci. Rep.*, **6**, 22469.
11. Eaton,M.L., Prinz,J.A., MacAlpine,H.K., Tretyakov,G., Kharchenko,P.V. and MacAlpine,D.M. (2011) Chromatin signatures of the Drosophila replication program. *Genome Res.*, **21**, 164–174.
12. Tardat,M., Brustel,J., Kirsh,O., Lefevbre,C., Callanan,M., Sardet,C. and Julien,E. (2010) The histone H4 Lys 20 methyltransferase PR-Set7 regulates replication origins in mammalian cells. *Nat. Cell Biol.*, **12**, 1086–1093.
13. Iizuka,M., Matsui,T., Takisawa,H. and Smith,M.M. (2006) Regulation of replication licensing by acetyltransferase Hbo1. *Mol. Cell. Biol.*, **26**, 1098–1108.
14. Wu,R., Wang,Z., Zhang,H., Gan,H. and Zhang,Z. (2017) H3K9me3 demethylase Kdm4d facilitates the formation of pre-initiative complex and regulates DNA replication. *Nucleic Acids Res.*, **45**, 169–180.
15. Chen,X., Liu,G. and Leffak,M. (2013) Activation of a human chromosomal replication origin by protein tethering. *Nucleic Acids Res.*, **41**, 6460–6474.
16. Liu,G., Malott,M. and Leffak,M. (2003) Multiple functional elements comprise a Mammalian chromosomal replicator. *Mol. Cell. Biol.*, **23**, 1832–1842.
17. Fu,H., Wang,L., Lin,C.M., Singhania,S., Bouhassira,E.E. and Aladjem,M.I. (2006) Preventing gene silencing with human replicators. *Nat. Biotechnol.*, **24**, 572–576.
18. Conner,A.L. and Aladjem,M.I. (2012) The chromatin backdrop of DNA replication: lessons from genetics and genome-scale analyses. *Biochim. Biophys. Acta*, **1819**, 794–801.
19. Majocchi,S., Aritonovska,E. and Mermod,N. (2014) Epigenetic regulatory elements associate with specific histone modifications to prevent silencing of telomeric genes. *Nucleic Acids Res.*, **42**, 193–204.
20. Aladjem,M.I. and Redon,C.E. (2016) Order from clutter: selective interactions at mammalian replication origins. *Nat. Rev. Genet.*, **18**, 101–116.
21. Huang,L., Fu,H., Lin,C.M., Conner,A., Zhang,Y. and Aladjem,M.I. (2011) Prevention of transcriptional silencing by a replicator-binding complex consisting of SWI/SNF, MeCP1 and hnRNP C1/C2. *Mol. Cell. Biol.*, **31**, 3472–3484.
22. Aladjem,M.I. (2007) Replication in context: dynamic regulation of DNA replication patterns in metazoans. *Nat. Rev. Genet.*, **8**, 588–600.
23. Flickinger,R.A. (2015) Possible role of H1 histone in replication timing. *Dev. Growth Differ.*, **57**, 1–9.
24. Bordone,L. and Guarente,L. (2005) Calorie restriction, SIRT1 and metabolism: understanding longevity. *Nat. Rev. Mol. Cell Biol.*, **6**, 298–305.
25. Oberdoerffer,P. and Sinclair,D.A. (2007) The role of nuclear architecture in genomic instability and ageing. *Nat. Rev. Mol. Cell Biol.*, **8**, 692–702.
26. Masri,S., Orozco-Solis,R., Aguilar-Arnal,L., Cervantes,M. and Sassone-Corsi,P. (2015) Coupling circadian rhythms of metabolism and chromatin remodelling. *Diabetes Obes. Metab.*, **17**(Suppl. 1), 17–22.
27. Carafa,V., Nebbioso,A. and Altucci,L. (2012) Sirtuins and disease: the road ahead. *Front. Pharmacol.*, **3**, 4.
28. Yuan,H., Su,L. and Chen,W.Y. (2013) The emerging and diverse roles of sirtuins in cancer: a clinical perspective. *Onco Targets Ther.*, **6**, 1399–1416.
29. Palacios DeBeer,M.A., Muller,U. and Fox,C.A. (2003) Differential DNA affinity specifies roles for the origin recognition complex in budding yeast heterochromatin. *Genes Dev.*, **17**, 1817–1822.
30. Fox,C.A. and Weinreich,M. (2008) Beyond heterochromatin: SIR2 inhibits the initiation of DNA replication. *Cell Cycle*, **7**, 3330–3334.
31. Fatoba,S.T., Tognetti,S., Berto,M., Leo,E., Mulvey,C.M., Godovac-Zimmermann,J., Pommier,Y. and Okorokov,A.L. (2013) Human SIRT1 regulates DNA binding and stability of the Mcm10 DNA replication factor via deacetylation. *Nucleic Acids Res.*, **41**, 4065–4079.
32. Wang,C., Chen,L., Hou,X., Li,Z., Kabra,N., Ma,Y., Nemoto,S., Finkel,T., Gu,W., Cress,W.D. *et al.* (2006) Interactions between E2F1 and SirT1 regulate apoptotic response to DNA damage. *Nat. Cell Biol.*, **8**, 1025–1031.

33. Wang,R.H., Lahusen,T.J., Chen,Q., Xu,X., Jenkins,L.M., Leo,E., Fu,H., Aladjem,M., Pommier,Y., Appella,E. *et al.* (2014) SIRT1 deacetylates TopBP1 and modulates intra-S-phase checkpoint and DNA replication origin firing. *Int. J. Biol. Sci.*, **10**, 1193–1202.
34. Liu,T., Lin,Y.H., Leng,W., Jung,S.Y., Zhang,H., Deng,M., Evans,D., Li,Y., Luo,K., Qin,B. *et al.* (2014) A divergent role of the SIRT1-TopBP1 axis in regulating metabolic checkpoint and DNA damage checkpoint. *Mol. Cell*, **56**, 681–695.
35. Sasaki,T., Maier,B., Koclega,K.D., Chruszcz,M., Gluba,W., Stukenberg,P.T., Minor,W. and Scrable,H. (2008) Phosphorylation regulates SIRT1 function. *PLoS One*, **3**, e4020.
36. Nasrin,N., Kaushik,V.K., Fortier,E., Wall,D., Pearson,K.J., de Cabo,R. and Bordone,L. (2009) JNK1 phosphorylates SIRT1 and promotes its enzymatic activity. *PLoS One*, **4**, e8414.
37. Guo,X., Williams,J.G., Schug,T.T. and Li,X. (2010) DYRK1A and DYRK3 promote cell survival through phosphorylation and activation of SIRT1. *J. Biol. Chem.*, **285**, 13223–13232.
38. Conrad,E., Polonio-Vallon,T., Meister,M., Matt,S., Bitomsky,N., Herbel,C., Liebl,M., Greiner,V., Kriznik,B., Schumacher,S. *et al.* (2016) HIPK2 restricts SIRT1 activity upon severe DNA damage by a phosphorylation-controlled mechanism. *Cell Death Differ.*, **23**, 110–122.
39. Luna,A., Aladjem,M.I. and Kohn,K.W. (2013) SIRT1/PARP1 crosstalk: connecting DNA damage and metabolism. *Genome Integr.*, **4**, 6.
40. O'Hagan,H.M., Wang,W., Sen,S., Destefano Shields,C., Lee,S.S., Zhang,Y.W., Clements,E.G., Cai,Y., Van Neste,L., Easwaran,H. *et al.* (2011) Oxidative damage targets complexes containing DNA methyltransferases, SIRT1, and polycomb members to promoter CpG Islands. *Cancer Cell*, **20**, 606–619.
41. Martin,M.M., Ryan,M., Kim,R., Zakas,A.L., Fu,H., Lin,C.M., Reinhold,W.C., Davis,S.R., Bilke,S., Liu,H. *et al.* (2011) Genome-wide depletion of replication initiation events in highly transcribed regions. *Genome Res.*, **21**, 1822–1832.
42. Fu,H., Martin,M.M., Regairaz,M., Huang,L., You,Y., Lin,C.M., Ryan,M., Kim,R., Shimura,T., Pommier,Y. *et al.* (2015) The DNA repair endonuclease Mus81 facilitates fast DNA replication in the absence of exogenous damage. *Nat. Commun.*, **6**, 6746.
43. Guo,X., Kesimer,M., Tolun,G., Zheng,X., Xu,Q., Lu,J., Sheehan,J.K., Griffith,J.D. and Li,X. (2012) The NAD(+)-dependent protein deacetylase activity of SIRT1 is regulated by its oligomeric status. *Sci. Rep.*, **2**, 640.
44. Tsuji,T., Ficarro,S.B. and Jiang,W. (2006) Essential role of phosphorylation of MCM2 by Cdc7/Dbf4 in the initiation of DNA replication in mammalian cells. *Mol. Biol. Cell*, **17**, 4459–4472.
45. Anglana,M., Apiou,F., Bensimon,A. and Debatisse,M. (2003) Dynamics of DNA replication in mammalian somatic cells: nucleotide pool modulates origin choice and interorigin spacing. *Cell*, **114**, 385–394.
46. Madireddy,A., Kosiyatrakul,S.T., Boisvert,R.A., Herrera-Moyano,E., Garcia-Rubio,M.L., Gerhardt,J., Vuono,E.A., Owen,N., Yan,Z., Olson,S. *et al.* (2016) FANCD2 facilitates replication through common fragile sites. *Mol. Cell*, **64**, 388–404.
47. Aranda,S., Laguna,A. and de la Luna,S. (2011) DYRK family of protein kinases: evolutionary relationships, biochemical properties, and functional roles. *FASEB J.*, **25**, 449–462.
48. Taira,N., Mimoto,R., Kurata,M., Yamaguchi,T., Kitagawa,M., Miki,Y. and Yoshida,K. (2012) DYRK2 priming phosphorylation of c-Jun and c-Myc modulates cell cycle progression in human cancer cells. *J. Clin. Invest.*, **122**, 859–872.
49. Nihira,N.T. and Yoshida,K. (2015) Engagement of DYRK2 in proper control for cell division. *Cell Cycle*, **14**, 802–807.
50. Mimoto,R., Taira,N., Takahashi,H., Yamaguchi,T., Okabe,M., Uchida,K., Miki,Y. and Yoshida,K. (2013) DYRK2 controls the epithelial-mesenchymal transition in breast cancer by degrading Snail. *Cancer Lett.*, **339**, 214–225.
51. Maddika,S. and Chen,J. (2009) Protein kinase DYRK2 is a scaffold that facilitates assembly of an E3 ligase. *Nat. Cell. Biol.*, **11**, 409–419.
52. Sirbu,B.M., McDonald,W.H., Dungrawala,H., Badu-Nkansah,A., Kavanaugh,G.M., Chen,Y., Tabb,D.L. and Cortez,D. (2013) Identification of proteins at active, stalled, and collapsed replication forks using isolation of proteins on nascent DNA (iPOND) coupled with mass spectrometry. *J. Biol. Chem.*, **288**, 31458–31467.
53. Chadha,G.S., Gambus,A., Gillespie,P.J. and Blow,J.J. (2016) Xenopus Mcm10 is a CDK-substrate required for replication fork stability. *Cell Cycle*, **15**, 2183–2195.
54. Smith,O.K. and Aladjem,M.I. (2014) Chromatin structure and replication origins: determinants of chromosome replication and nuclear organization. *J. Mol. Biol.*, **426**, 3330–3341.
55. Mechali,M., Yoshida,K., Coulombe,P. and Pasero,P. (2013) Genetic and epigenetic determinants of DNA replication origins, position and activation. *Curr. Opin. Genet. Dev.*, **23**, 124–131.
56. Wang,Y., Khan,A., Marks,A.B., Smith,O.K., Giri,S., Lin,Y.C., Creager,R., MacAlpine,D.M., Prasanth,K.V., Aladjem,M.I. *et al.* (2016) Temporal association of ORCA/LRWD1 to late-firing origins during G1 dictates heterochromatin replication and organization. *Nucleic Acids Res.*, **45**, 2490–2502.
57. Devbhandari,S., Jiang,J., Kumar,C., Whitehouse,I. and Remus,D. (2016) Chromatin constrains the initiation and elongation of DNA replication. *Mol. Cell*, **65**, 131–141.
58. Kurat,C.F., Yeeles,J.T., Patel,H., Early,A. and Diffley,J.F. (2016) Chromatin controls DNA replication origin selection, lagging-strand synthesis, and replication fork rates. *Mol. Cell*, **65**, 117–130.
59. Miotto,B. and Struhl,K. (2010) HBO1 histone acetylase activity is essential for DNA replication licensing and inhibited by Geminin. *Mol. Cell*, **37**, 57–66.
60. Kuo,A.J., Song,J., Cheung,P., Ishibe-Murakami,S., Yamazoe,S., Chen,J.K., Patel,D.J. and Gozani,O. (2012) The BAH domain of ORC1 links H4K20me2 to DNA replication licensing and Meier-Gorlin syndrome. *Nature*, **484**, 115–119.
61. Rivera-Mulia,J.C. and Gilbert,D.M. (2016) Replicating large genomes: divide and conquer. *Mol. Cell*, **62**, 756–765.
62. Blow,J.J., Ge,X.Q. and Jackson,D.A. (2011) How dormant origins promote complete genome replication. *Trends Biochem. Sci.*, **36**, 405–414.
63. Kawabata,T., Luebben,S.W., Yamaguchi,S., Ilves,I., Matise,I., Buske,T., Botchan,M.R. and Shima,N. (2011) Stalled fork rescue via dormant replication origins in unchallenged S phase promotes proper chromosome segregation and tumor suppression. *Mol. Cell*, **41**, 543–553.
64. McBurney,M.W., Yang,X., Jardine,K., Hixon,M., Boekelheide,K., Webb,J.R., Lansdorp,P.M. and Lemieux,M. (2003) The mammalian SIR2alpha protein has a role in embryogenesis and gametogenesis. *Mol. Cell. Biol.*, **23**, 38–54.
65. Chini,C.C., Espindola-Netto,J.M., Mondal,G., Guerrico,A.M., Nin,V., Escande,C., Sola-Penna,M., Zhang,J.S., Billadeau,D.D. and Chini,E.N. (2016) SIRT1-activating compounds (STAC) negatively regulate pancreatic cancer cell growth and viability through a SIRT1 lysosomal-dependent pathway. *Clin. Cancer Res.*, **22**, 2496–2507.
66. Wang,R.H., Sengupta,K., Li,C., Kim,H.S., Cao,L., Xiao,C., Kim,S., Xu,X., Zheng,Y., Chilton,B. *et al.* (2008) Impaired DNA damage response, genome instability, and tumorigenesis in SIRT1 mutant mice. *Cancer Cell*, **14**, 312–323.
67. Herranz,D., Munoz-Martin,M., Canamero,M., Mulero,F., Martinez-Pastor,B., Fernandez-Capetillo,O. and Serrano,M. (2010) Sirt1 improves healthy ageing and protects from metabolic syndrome-associated cancer. *Nat. Commun.*, **1**, 3.
68. Simic,P., Williams,E.O., Bell,E.L., Gong,J.J., Bonkowski,M. and Guarente,L. (2013) SIRT1 suppresses the epithelial-to-mesenchymal transition in cancer metastasis and organ fibrosis. *Cell Rep.*, **3**, 1175–1186.
69. Singh,S.K., Williams,C.A., Klarmann,K., Burkett,S.S., Keller,J.R. and Oberdoerffer,P. (2013) Sirt1 ablation promotes stress-induced loss of epigenetic and genomic hematopoietic stem and progenitor cell maintenance. *J. Exp. Med.*, **210**, 987–1001.
70. Ibarra,A., Schwob,E. and Mendez,J. (2008) Excess MCM proteins protect human cells from replicative stress by licensing backup origins of replication. *Proc. Natl. Acad. Sci. U.S.A.*, **105**, 8956–8961.
71. Woodward,A.M., Gohler,T., Luciani,M.G., Oehlmann,M., Ge,X., Gartner,A., Jackson,D.A. and Blow,J.J. (2006) Excess Mcm2-7 license dormant origins of replication that can be used under conditions of replicative stress. *J. Cell Biol.*, **173**, 673–683.
72. Kim,R., Smith,O.K., Wong,W.C., Ryan,A.M., Ryan,M.C. and Aladjem,M.I. (2015) ColoWeb: a resource for analysis of colocalization of genomic features. *BMC Genomics*, **16**, 1345.